

# Modeling and simulation of nematic LCE rods

Sören Bartels<sup>1\*</sup>, Max Griehl<sup>2§</sup>, Jakob Keck<sup>3\*</sup>, and Stefan Neukamm<sup>4§</sup>

<sup>\*</sup>Department of Applied Mathematics, University of Freiburg

<sup>§</sup>Faculty of Mathematics, Technische Universität Dresden

May 31, 2022

## Abstract

We introduce a nonlinear, one-dimensional bending-twisting model for an inextensible bi-rod that is composed of a nematic liquid crystal elastomer. The model combines an elastic energy that is quadratic in curvature and torsion with a Frank-Oseen energy for the liquid crystal elastomer. Moreover, the model features a nematic-elastic coupling that relates the crystalline orientation with a spontaneous bending-twisting term. We show that the model can be derived as a  $\Gamma$ -limit from three-dimensional nonlinear elasticity. Moreover, we introduce a numerical scheme to compute critical points of the bending-twisting model via a discrete gradient flow. We present various numerical simulations that illustrate the rich mechanical behavior predicted by the model. The numerical experiments reveal good stability and approximation properties of the method.

**Keywords:** dimension reduction, nonlinear elasticity, nonlinear rods, liquid crystal elastomer, constrained finite element method.

**MSC-2020:** 74B20; 76A15; 74K10; 65N30; 74-10.

## Contents

<b>1</b>	<b>Introduction</b>	<b>2</b>
<b>2</b>	<b>A bi-rod model for nematic LCEs and its derivation</b>	<b>3</b>
2.1	The one-dimensional model . . . . .	3
2.2	The three-dimensional model and $\Gamma$ -convergence . . . . .	4
2.3	Definition and evaluation of the effective coefficients . . . . .	7
2.4	The special case of an isotropic material with circular cross-section . . . . .	9
<b>3</b>	<b>Simulation and model exploration</b>	<b>10</b>
3.1	Numerical minimization by a discrete gradient flow . . . . .	12
3.2	Numerical experiments . . . . .	13
<b>4</b>	<b>Proofs</b>	<b>21</b>
4.1	Compactness – Proof of Theorem 2.1 (a) and Proposition 2.2 (a) . . . . .	21
4.2	Lower bound – Proof of Theorem 2.1 (b) . . . . .	22
4.3	Upper bound – Proofs of Theorem 2.1 (c) and Proposition 2.2 (b) . . . . .	22
4.4	Anchoring – Proof of Proposition 2.3 . . . . .	24
4.5	Proofs of Lemmas 2.7, 2.9, 2.10, and 2.11 . . . . .	25

---

<sup>1</sup>bartels@mathematik.uni-freiburg.de

<sup>2</sup>max.griehl@tu-dresden.de

<sup>3</sup>jakob.keck@math.uni-freiburg.de

<sup>4</sup>stefan.neukamm@tu-dresden.de

# 1 Introduction

Nematic liquid crystal elastomers (LCE) are nonlinearly elastic materials that feature an additional orientational internal degree of freedom. They are composed of a polymer network with incorporated liquid crystals—rod-like molecules that tend to align in a nematic phase. Nematic LCE feature a nematic-elastic coupling between the orientation of the liquid crystals and the elastic properties of the polymer network. More specifically, the material tends to stretch in the direction parallel to the liquid crystal orientation and shrinks in orthogonal directions. Furthermore, it is possible to tweak the orientation of the liquid crystals by fields and to (de)activate the nematic-elastic coupling by external stimuli (e.g., temperature). For this reasons, nematic LCE exhibit interesting mechanical properties (e.g., thermo-mechanical coupling [BCZ11, WT07] or soft elasticity [KF91, KF95]), and are used to design active materials, see [WB15, WBS<sup>+</sup>16, vMJZ18]. In this context, slender structure such as thin films and rods are of interest. In recent years nonlinear models for thin films and rods made of nematic LCE have also been intensively studied from a mathematical perspective. In particular, the derivation of lower-dimensional models from three-dimensional models has been discussed, e.g., see [CDD02b, CDD02a, PLB18, PKWB18, CPB15, AD17b, AD17a, ALL17, ADK17, BNS20], and reliable numerical schemes have been developed, e.g., see [BP21, BGN<sup>+</sup>21, BBMN18, BBN17, San10, SNB16, LTMR92, BWR<sup>+</sup>08] for numerical methods for slender structures, [NWZ17a, NRV20, NWZ17b, BNW20, Wal20] for LCE and director fields, and [BGN<sup>+</sup>22] for models that combination thin-film mechanics and director fields.

Our paper is devoted to the modeling and simulation of nonlinear bi-rods that are composed of nematic LCE and a usual nonlinear elastic material. Starting from a three-dimensional nonlinear model that invokes a standard energy functional from nonlinear elasticity, a Frank-Oseen energy for the LCE material, and a nematic-elastic coupling term, we derive via  $\Gamma$ -convergence a model for an inextensible rod that is capable to describe large bending and twisting deformations, and a coupling mechanism that relates the local orientation of the LCE with a spontaneous curvature/torsion-term. In contrast to other works, e.g., [GMAM22], in our model the director field is not prescribed but an additional degree of freedom of the model; moreover, the derivation is ansatz-free in the sense of  $\Gamma$ -convergence. It is based on the one hand on the recently introduced approach in [BGN<sup>+</sup>22] where the derivation of nematic LCE plates is studied, and on the other hand, on [Neu12, BNS20] where the simultaneous homogenization and dimension reduction of prestrained rods is analyzed as an extension of the seminal work [MM03].

Our effective one-dimensional description of LCE rods allows for efficient numerical simulations of complex problem settings. We follow [BR20] and use standard  $C^0$  and  $C^1$  conforming finite element spaces that are subordinated to a partitioning of the straight reference configuration to approximate director fields and the bending deformation, respectively. Geometric constraints such as the conditions for the material frame are imposed at nodes of the partitioning via suitable linearizations and penalty terms. Similarly, the discretization of the unit-length constraint for the director field describing the LCE orientation is imposed at the nodes. We then use a semi-implicit gradient descent method to decrease the one-dimensional energy functional from a given initial state to obtain stationary configurations via sequences of linear problems with simple system matrices. Our experiments show how a periodic bending behaviour can be controlled in a quasi-static setting via a time-dependent external field. Our simulations also illustrate how internal material parameters, that can be changed via external stimuli, affect the bending behavior in the case of compressive, twist-inducing boundary conditions. The numerical experiments reveal good stability and approximation properties of the iterative method and the devised discretization scheme. They lead to meaningful results within minutes for an

elementary implementation on standard desktop computers.

The paper is structured as follows. In Section 2 we first introduce the one-dimensional bending-twisting model. We then introduce a three-dimensional nonlinear elasticity model and show that it  $\Gamma$ -converges to the one-dimensional model, see Section 2.2. The effective coefficients of the one-dimensional depend on the original material, the geometry of the cross-section and the domain occupied by the LCE. In Section 2.3 we present their definition and derive simplified formulas that hold in special settings. In Section 3 we introduce a discretization of the one-dimensional model minimization problem via a discrete gradient flow, and we explore the model via numerical simulations. All proofs are presented in Section 4.

## 2 A bi-rod model for nematic LCEs and its derivation

In this section we introduce a one-dimensional bending-twisting model that describes an inextensible rod that is composed of a nematic LCE and a nonlinearly elastic material, and we explain its derivation from three-dimensional nonlinear elasticity via  $\Gamma$ -convergence, see Section 2.2 below.

### 2.1 The one-dimensional model

We denote by  $\omega := (0, L)$  the reference domain of the rod. We describe a configuration of the rod by a triplet  $(y, R, n)$  satisfying

$$\begin{aligned} y &\in H^2(\omega; \mathbb{R}^3), \quad R \in H^1(\omega; \mathbb{R}^{3 \times 3}), \quad n \in H^1(\omega; \mathbb{R}^3) \\ \text{such that for a.e. } x_1 \in \omega, \quad &\partial_1 y(x_1) = R(x_1)e_1, \quad R(x_1) \in \text{SO}(3), \quad |n(x_1)| = 1. \end{aligned} \quad (1)$$

Here,  $y$  describes the deformation of the rod and  $R$  the deformation of an associated orthonormal frame. The field  $n$  describes the orientation of the liquid crystals in global coordinates. We denote by

$$\mathcal{A} := \{(y, R, n) : (y, R, n) \text{ satisfies (1)}\}$$

the set of all *rod configurations* and call a pair  $(y, R)$  satisfying (1) a *framed curve*. We consider the energy functional  $\mathcal{E} : \mathcal{A} \rightarrow \mathbb{R}$  defined by

$$\begin{aligned} \mathcal{E}(y, R, n) &:= \int_{\omega} \bar{Q} \left( R^\top \partial_1 R + \bar{r} K_{\text{pre}} \left( \frac{1}{3} I - \hat{n} \otimes \hat{n} \right) \right) + \bar{r}^2 E_{\text{res}} \left( \frac{1}{3} I - \hat{n} \otimes \hat{n} \right) dx_1 \\ &\quad + \kappa^2 \int_{\omega} |\partial_1 n|^2 dx', \quad \text{where } \hat{n} := R^\top n, \end{aligned} \quad (2)$$

where

- $\bar{Q} : \mathbb{R}_{\text{skew}}^{3 \times 3} \rightarrow \mathbb{R}$  is a positive definite quadratic form that describes the bending-twisting energy; here and below,  $\mathbb{R}_{\text{skew}}^{3 \times 3}$  denotes the space of skew-symmetric matrices in  $\mathbb{R}^{3 \times 3}$ .
- $K_{\text{pre}} : \mathbb{R}_{\text{dev}}^{3 \times 3} \rightarrow \mathbb{R}_{\text{skew}}^{3 \times 3}$  is a linear map that describes the contribution of the nematic-elastic coupling that leads to spontaneous bending and twisting of the rod; here and below,  $\mathbb{R}_{\text{dev}}^{3 \times 3}$  denotes the space of symmetric matrices in  $\mathbb{R}^{3 \times 3}$  with vanishing trace.
- $E_{\text{res}} : \mathbb{R}_{\text{dev}}^{3 \times 3} \rightarrow \mathbb{R}$  is a positive, semi-definite quadratic form that describes a residual energy that cannot be accommodated by bending or twisting of the rod.
- $\bar{r} \in \mathbb{R}$  is a model parameter related to the strength of the nematic-elastic coupling.

- $\kappa > 0$  is a model parameter that is related to the scaling of the physical diameter of the rod, the shear modulus of the elastomer and the Frank elastic constant of the nematic LCE.

As we shall explain next, this model can be derived as a zero-thickness  $\Gamma$ -limit from a three-dimensional rod composed of an elastic material and an LCE-material. In this context, the precise definition of  $\bar{Q}$  and  $K_{\text{pre}}$  depends on the considered material, the geometry of the cross-section of the rod and the geometry of the subdomain that is occupied by the nematic LCE material, see Definition 2.6.

## 2.2 The three-dimensional model and $\Gamma$ -convergence

The starting point of the derivation is the following three-dimensional situation: We consider an elastic composite material that occupies the three-dimensional, rod-like domain  $\Omega_h := \omega \times hS$ , where  $0 < h \ll 1$  denotes a (non-dimensionalized) thickness of the rod,  $S \subset \mathbb{R}^2$  the rescaled cross-section, and  $\omega := (0, L)$  the mid-line of the rod. We assume that

$$\begin{aligned} S \subset \mathbb{R}^2 \text{ is a simply connected, Lipschitz domain,} \\ \text{satisfying } \int_S x_2 d\bar{x} = \int_S x_3 d\bar{x} = \int_S x_2 x_3 d\bar{x} = 0. \end{aligned} \quad (3)$$

Here and below, we use the notation  $x = (x_1, \bar{x}) \in \mathbb{R}^3$  and  $\bar{x} = (x_2, x_3) \in \mathbb{R}^2$ . We note that the symmetry condition in (3) is not a restriction, since it can always be achieved by rotating and translating  $S$ . We assume that the rod is composed of a conventional elastic material and a nematic LCE. The latter occupies the subbody  $\Omega_{0,h} := \omega \times (hS_0)$  where  $S_0 \subset S$  denotes a subdomain of the cross-section. We assume that

$$S_0 \subset S \text{ is a simply connected, Lipschitz domain such that } |S_0| > 0 \text{ and } |S \setminus S_0| > 0. \quad (4)$$

To study the limit  $h \rightarrow 0$ , it is convenient to work with the rescaled domain  $\Omega := \omega \times S$  (resp. the rescaled subdomain  $\Omega_0 := \omega \times S_0$ ). We therefore describe the deformation of the rod by a mapping  $y_h : H^1(\Omega; \mathbb{R}^3)$ , and the orientation of the LCE by a director field  $n_h \in H^1(\Omega_0; \mathbb{S}^2)$ . Here and below,  $\mathbb{S}^2$  denotes unit-sphere in  $\mathbb{R}^3$ . We consider the energy functional

$$\begin{aligned} \mathcal{E}_h(y_h, n_h) := & \frac{1}{h^2|S|} \int_{\Omega \setminus \Omega_0} W(\bar{x}, \nabla_h y_h(x)) dx + \frac{1}{h^2|S|} \int_{\Omega_0} W(\bar{x}, L_h(n_h(x))^{-\frac{1}{2}} \nabla_h y_h(x)) dx \\ & + \frac{\kappa^2}{|S_0|} \int_{\Omega_0} |\nabla_h n_h(x) (\nabla_h y_h(x))^{-1}|^2 \det(\nabla_h y_h(x)) dx. \end{aligned} \quad (5)$$

The first integral is the elastic energy stored in the deformed material with reference configuration  $\Omega \setminus \Omega_0$ . Here,  $\nabla_h := (\partial_1, \frac{1}{h} \bar{\nabla})$ ,  $\bar{\nabla} := (\partial_2, \partial_3)$  denotes the scaled gradient which emerges when passing from  $\Omega_h$  to  $\Omega$ . The second integral is the elastic energy of the nematic LCE. It invokes the step-length tensor

$$L_h : \mathbb{S}^2 \rightarrow \mathbb{R}_{\text{sym}}^{3 \times 3}, \quad L_h(n) := (1 + h\bar{r})^{-\frac{1}{3}} (I + h\bar{r}n \otimes n),$$

which has been introduced by [BTW93] to model the elastic-nematic coupling. The last integral is the (one-constant approximation of the) Frank-Oseen energy pulled back to the reference configuration. As already mentioned,  $\bar{r} \in \mathbb{R}$  and  $\kappa > 0$  denote model parameters.

We assume that the stored energy function  $W : S \times \mathbb{R}^{3 \times 3} \rightarrow [0, \infty]$  is Borel-measurable and satisfies for some  $q > 4$  and  $C > 0$ , and for all  $F \in \mathbb{R}^{3 \times 3}$  and a.e.  $\bar{x} \in S$ ,

$$W(\bar{x}, RF) = W(\bar{x}, F) \quad \text{for all } R \in \text{SO}(3), \quad (\text{W1})$$

$$W(\bar{x}, F) \geq \frac{1}{C} \text{dist}^2(F, \text{SO}(3)) \text{ and } W(\bar{x}, I) = 0, \quad (\text{W2})$$

$$W(\bar{x}, \cdot) \text{ is } C^2 \text{ in } \{F \in \mathbb{R}^{3 \times 3} : \text{dist}(F, \text{SO}(3)) < \frac{1}{C}\}, \quad (\text{W3})$$

$$W(\bar{x}, F) \geq \begin{cases} \frac{1}{C} \max\{|F|^q, \det(F)^{-\frac{q}{2}}\} - C & \text{if } \det F > 0, \\ +\infty & \text{else.} \end{cases} \quad (\text{W4})$$

The stored energy function thus describes a frame indifferent, cf. (W1), material with a stress-free, non-degenerate reference configuration, cf. (W2). Furthermore, by (W3) the material law is linearizable at identity and the linearization is Korn-elliptic, i.e., the quadratic form defined by

$$Q : S \times \mathbb{R}^{3 \times 3} \rightarrow \mathbb{R}, \quad Q(\bar{x}, G) := \frac{1}{2} \nabla^2 W(\bar{x}, I) G \cdot G, \quad (6)$$

vanishes on  $\mathbb{R}_{\text{skew}}^{3 \times 3}$  and is positive definite on  $\mathbb{R}_{\text{sym}}^{3 \times 3}$ . We remark that (5) is precisely the analogue for rods of the energy functional considered in [BGN<sup>+</sup>22] where the a bending model for LCE-plates is studied. The next theorem shows that  $\mathcal{E}_h$   $\Gamma$ -converges as  $h \rightarrow 0$  to the one-dimensional limiting model (2):

**Theorem 2.1** (Derivation via dimension reduction). *Let the cross-section  $S$  and  $S_0 \subseteq S$  satisfy (3), (4), and let  $W$  satisfy (W1) – (W4). Let  $\mathcal{E} : \mathcal{A} \rightarrow \mathbb{R}$  be defined by (2) with  $\bar{Q}$ ,  $K_{\text{pre}}$  and  $E_{\text{res}}$  given by Definition 2.6. Then the following properties hold:*

(a) (Compactness). *Suppose  $\limsup_{h \rightarrow 0} \mathcal{E}_h(y_h, n_h) < \infty$ . Then there exists  $(y, R, n) \in \mathcal{A}$  such that for a subsequence (not relabeled), we have*

$$(y_h - \oint_{\Omega} y_h, \nabla_h y_h) \rightarrow (y, R) \quad \text{in } L^2, \quad (7)$$

$$n_h \rightarrow n \quad \text{in } L^2. \quad (8)$$

(b) (Lower bound). *Let  $(y_h, n_h) \subset H^1(\Omega; \mathbb{R}^3) \times H^1(\Omega_0; \mathbb{S}^2)$  and  $(y, R, n) \in \mathcal{A}$ . Suppose that  $(y_h, \nabla_h y_h, n_h) \rightarrow (y, R, n)$  strongly in  $L^2$ . Then*

$$\liminf_{h \rightarrow 0} \mathcal{E}_h(y_h, n_h) \geq \mathcal{E}(y, R, n).$$

(c) (Upper bound). *Let  $(y, R, n) \in \mathcal{A}$ . Then there exists a sequence  $(y_n, n_n) \subset H^1(\Omega; \mathbb{R}^3) \times H^1(\Omega_0; \mathbb{S}^2)$  such that  $(y_n, \nabla_h y_n, n_n) \rightarrow (y, R, n)$  strongly in  $L^2$  and*

$$\lim_{h \rightarrow 0} \mathcal{E}_h(y_h, n_h) = \mathcal{E}(y, R, n).$$

For the proof see Section 4.

We can take also clamped boundary conditions for the deformation into account:

**Proposition 2.2** (Clamped boundary conditions). *Let  $y_{bc} \in H^2(\omega; \mathbb{R}^3)$ ,  $R_{bc} \in H^1(\omega; \text{SO}(3))$ , and suppose that  $\partial_1 y_{bc} = R_{bc} e_1$ .*

(a) Consider the situation of Theorem 2.1 (a) and additionally suppose that

$$y_h(0, \bar{x}) = y_{bc}(0) + hR_{bc}(0)\bar{x} \quad \text{a.e. in } S, \quad (9)$$

where here and below, we write  $\bar{x}$  for the map  $S \ni \bar{x} \mapsto (0, \bar{x})^\top \in \mathbb{R}^3$ . Then there exists  $(y, R, n) \in \mathcal{A}$  with

$$(y(0), R(0)) = (y_{bc}(0), R_{bc}(0)), \quad (10)$$

such that for a subsequence (not relabeled), we have

$$(y_h, \nabla_h y_h, n_h) \rightarrow (y, R, n) \quad \text{in } L^2. \quad (11)$$

(b) Consider the situation of Theorem 2.1 (c) and suppose that  $(y, R, n) \in \mathcal{A}$  satisfies (10). Then there exists a sequence  $(y_n, n_h) \subset H^1(\Omega; \mathbb{R}^3) \times H^1(\Omega_0; \mathbb{S}^2)$  that satisfies (9) such that  $(y_h, \nabla_h y_h, n_h) \rightarrow (y, R, n)$  strongly in  $L^2$  and

$$\lim_{h \rightarrow 0} \mathcal{E}_h(y_h, n_h) = \mathcal{E}(y, R, n).$$

For the proof see Section 4. Next, we discuss soft anchoring conditions for the director  $n_h$ .

They come in the form of an additional contribution to the energy functional that penalizes deviations of the director  $n_h$  from a prescribed configuration  $\hat{n}_{bc}$ . In this context, it is natural to describe the director in local coordinates. In the following we first introduce a general form of a soft anchoring condition for the three-dimensional model: Let  $|\cdot|_a$  denote a semi-norm on  $\mathbb{R}^3$ , and let  $\rho \in L^1(\Omega_0)$  denote a non-negative weight and set  $\bar{\rho}(x_1) := \int_{S_0} \rho(x_1, \bar{x}) d\bar{x}$ . For  $(y_h, n_h)$  with  $\mathcal{E}_h(y_h, n_h) < \infty$  and  $\hat{n}_{bc} \in H^1(\omega; \mathbb{S}^2)$  define

$$\mathcal{G}_h(y_h, n_h; \hat{n}_{bc}) := \int_{\Omega_0} \left| \frac{\nabla_h y_h^\top n_h}{|\nabla_h y_h^\top n_h|} - \hat{n}_{bc} \right|_a^2 \rho dx.$$

Furthermore, for  $(y, R, n) \in \mathcal{A}$  and  $\hat{n}_{bc} \in H^1(\omega; \mathbb{S}^2)$  define

$$\begin{aligned} \mathcal{G}_{\text{weak}}(y, R, n; \hat{n}_{bc}) &:= \int_{\omega} \left| R^\top n - \hat{n}_{bc} \right|_a^2 \bar{\rho} dx_1, \\ \mathcal{G}_{\text{strong}}(y, R, n; \hat{n}_{bc}) &:= \begin{cases} 0 & \text{if } |R^\top n - \hat{n}_{bc}|_a^2 \bar{\rho} = 0 \text{ a.e. in } \omega, \\ \infty & \text{else.} \end{cases} \end{aligned}$$

**Proposition 2.3** (Derivation of anchorings). (a) The statements of Theorem 2.1 hold with  $(\mathcal{E}_h, \mathcal{E})$  being replaced by  $(\mathcal{E}_h + \mathcal{G}_h, \mathcal{E} + \mathcal{G}_{\text{weak}})$ .

(b) Let  $0 < \beta < 1$ . The statements of Theorem 2.1 hold with  $(\mathcal{E}_h, \mathcal{E})$  being replaced by  $(\mathcal{E}_h + h^{-\beta} \mathcal{G}_h, \mathcal{E} + \mathcal{G}_{\text{strong}})$ .

For the proof see Section 4.

**Example 2.1.** (a) (Full anchoring). In the case  $|\cdot|_a := |\cdot|$  and  $\rho \equiv |S_0|^{-1}$  we obtain

$$\mathcal{G}_{\text{weak}}(y, R, n; \hat{n}_{bc}) = \int_{\omega} \left| R^\top n - \hat{n}_{bc} \right|^2 dx_1,$$

which penalizes deviations of the director from  $\hat{n}_{bc}$ . The corresponding strong anchoring enforces the director (in local coordinates) to be equal to  $\hat{n}_{bc}$  a.e. in  $\omega$ .

(b) (Tangentiality). Consider  $|\xi|_a^2 := (\xi \cdot e_2)^2 + (\xi \cdot e_3)^2$ ,  $\rho \equiv |S_0|^{-1}$  and  $\hat{n}_{bc} := e_1$ . We obtain

$$\mathcal{G}_{\text{weak}}(y, R, n; \hat{n}_{bc}) = \int_{\omega} (n \cdot R e_2)^2 + (n \cdot R e_3)^2 dx_1,$$

which penalizes the non-tangential components of the director. The corresponding strong anchoring enforces the director (in local coordinates) to be tangential, i.e.,  $n = y'$ .

(c) (Normality). Consider  $|\xi|_a^2 := (\xi \cdot e_1)^2$ ,  $\rho \equiv |S_0|^{-1}$  and  $\hat{n}_{bc} := e_2$ . We obtain

$$\mathcal{G}_{\text{weak}}(y, R, n; \hat{n}_{bc}) = \int_{\omega} (n \cdot y')^2 dx_1,$$

which penalizes the tangential components of the director. The corresponding strong anchoring enforces the director (in local coordinates) to be normal to the tangent.

### 2.3 Definition and evaluation of the effective coefficients

In the following we present the definition of the effective coefficients  $\bar{Q}$ ,  $K_{\text{eff}}$  and  $E_{\text{res}}$ . We first define the effective coefficients abstractly based on a projection scheme introduced in [BNS20]. We then characterize the coefficients with help of cell-problems and correctors. Finally, we derive more explicit formulas in the special case of an isotropic material. Throughout this section we assume that  $W$  satisfies (W1) – (W4) and that  $Q$  is defined by (6).

For the abstract definition let  $\mathbb{H} := L^2(S; \mathbb{R}_{\text{sym}}^{3 \times 3})$  denote the Hilbert space with scalar product

$$(\Psi, \Phi)_Q := \frac{1}{2} \int_S \mathbb{L}(\bar{x}) \Psi(\bar{x}) \cdot \Phi(\bar{x}) d\bar{x},$$

where  $\frac{1}{2} \mathbb{L}(\bar{x}) G \cdot G' = \frac{1}{2} \nabla^2 W(\bar{x}, I) G \cdot G'$  for all  $G, G' \in \mathbb{R}^{3 \times 3}$ . Note that the associated norm is given by  $\|\Psi\|_Q^2 = \int_S Q(\bar{x}, \Psi(\bar{x})) d\bar{x}$ . We consider the subspaces

$$\begin{aligned} \mathbb{H}_{\text{rel}} &:= \left\{ S \ni \bar{x} \mapsto a e_1 \otimes e_1 + \text{sym}(0, \bar{\nabla} \varphi(\bar{x})) : a \in \mathbb{R}, \varphi \in H^1(S; \mathbb{R}^3) \right\}, \\ \mathbb{H}_{\text{micro}} &:= \left\{ S \ni \bar{x} \mapsto \text{sym}((K \bar{x}) \otimes e_1) + \chi(\bar{x}) : K \in \mathbb{R}_{\text{skew}}^{3 \times 3}, \chi \in \mathbb{H}_{\text{rel}} \right\}. \end{aligned}$$

With help of Korn's inequality we deduce the following statement (whose elementary proof we leave to the reader):

**Lemma 2.4.** *Let  $H_{\text{av}}^1(S; \mathbb{R}^3)$  denote the space of functions  $\varphi \in H^1(S; \mathbb{R}^3)$  satisfying*

$$\int_S \varphi = 0 \text{ and } \int_S \partial_3 \varphi_2 - \partial_2 \varphi_3 d\bar{x} = 0.$$

*Then  $H_{\text{av}}^1(S; \mathbb{R}^3)$  equipped with the norm  $\varphi \mapsto (\int_S |\text{sym}(0, \bar{\nabla} \varphi)|^2 d\bar{x})^{\frac{1}{2}}$  is a Hilbert space. Furthermore, the map*

$$\mathbb{R} \times H_{\text{av}}^1(S; \mathbb{R}^3) \ni (a, \varphi) \mapsto \text{sym}(a e_1, \bar{\nabla} \varphi) \in \mathbb{H}_{\text{rel}}$$

*is an isomorphism.*

The previous lemma implies that  $\mathbb{H}_{\text{rel}}$  and  $\mathbb{H}_{\text{micro}}$  are closed subspaces of  $\mathbb{H}$ . Thus, the subspaces  $\mathbb{H}_{\text{res}}$  and  $\mathbb{H}_{\text{macro}}$  defined by the  $(\cdot, \cdot)_Q$ -orthogonal decompositions

$$\mathbb{H} = \mathbb{H}_{\text{micro}} \oplus \mathbb{H}_{\text{res}}, \quad \mathbb{H}_{\text{micro}} = \mathbb{H}_{\text{macro}} \oplus \mathbb{H}_{\text{rel}},$$

are closed as well. In the following, we write  $P_X$  for the orthogonal projection onto a closed subspace  $X \subset \mathbb{H}$ .

We recall the following result, which is a special case of [BNS20, Lemma 2.10]:

**Lemma 2.5.** *The map*

$$\mathbf{E} : \mathbb{R}_{\text{skew}}^{3 \times 3} \rightarrow \mathbb{H}_{\text{macro}}, \quad \mathbf{E}(K) := P_{\mathbb{H}_{\text{macro}}} \left( \text{sym}((K\bar{\mathbf{x}}) \otimes e_1) \right)$$

*is a linear isomorphism.*

We are now in position to define the effective coefficients as follows:

**Definition 2.6** (Effective coefficients).

$$\begin{aligned} \bar{Q} : \mathbb{R}_{\text{skew}}^{3 \times 3} &\rightarrow \mathbb{R}, & \bar{Q}(K) &:= \|\mathbf{E}(K)\|_Q^2, \\ K_{\text{pre}} : \mathbb{R}_{\text{dev}}^{3 \times 3} &\rightarrow \mathbb{R}_{\text{skew}}^{3 \times 3}, & K_{\text{pre}}(U) &:= (\mathbf{E}^{-1} \circ P_{\mathbb{H}_{\text{macro}}}) \left( \frac{1}{2} \mathbf{1}_{S_0} U \right), \\ E_{\text{res}} : \mathbb{R}_{\text{dev}}^{3 \times 3} &\rightarrow \mathbb{R}, & E_{\text{res}}(U) &:= \|P_{\mathbb{H}_{\text{res}}} \left( \frac{1}{2} \mathbf{1}_{S_0} U \right)\|_Q^2. \end{aligned}$$

The definition is motivated by the following relaxation result:

**Lemma 2.7** (Relaxation formula). *Let  $K \in \mathbb{R}_{\text{skew}}^{3 \times 3}$  and  $U \in \mathbb{R}_{\text{dev}}^{3 \times 3}$ . Then*

$$\begin{aligned} \inf_{\chi \in \mathbb{H}_{\text{rel}}} \int_S Q \left( \bar{\mathbf{x}}, \text{sym}((K\bar{\mathbf{x}}) \otimes e_1) + \frac{\bar{r}}{2} \mathbf{1}_{S_0} U + \chi \right) \\ = \bar{Q}(K + \bar{r} K_{\text{pre}}(U)) + \bar{r}^2 E_{\text{res}}(U). \end{aligned}$$

Thanks to the assumptions on  $W$  and  $S$  we obtain the following properties:

**Lemma 2.8.** *The maps  $\bar{Q}$  and  $E_{\text{res}}$  are quadratic, and  $K_{\text{pre}}$  is linear. Moreover, there exists  $C > 0$  only depending on  $W$  and  $S$  such that*

$$\begin{aligned} \frac{1}{C} |K|^2 &\leq \bar{Q}(K) \leq C |K|^2, \\ 0 &\leq E_{\text{res}}(U) \leq C |U|^2, \\ |K_{\text{pre}}(U)| &\leq C |U|. \end{aligned}$$

We omit the proof, since it is similar to [BGN<sup>+</sup>22, Lemma 2.6].

Next, we introduce a scheme to evaluate these quantities. The scheme invokes 3 + 5 correctors that only depend on  $Q$ ,  $S$  and  $S_0$ , and are defined with help of linear elliptic systems on the domain  $S$ . We start by representing the effective coefficients in coordinates. To that end, we consider the following orthonormal basis of  $\mathbb{R}_{\text{dev}}^{3 \times 3}$ ,

$$\begin{aligned} U_1 &:= \sqrt{2} \text{sym}(e_3 \otimes e_2), & U_2 &:= \sqrt{2} \text{sym}(e_2 \otimes e_1), & U_3 &:= \sqrt{2} \text{sym}(e_3 \otimes e_1), \\ U_4 &:= \sqrt{\frac{2}{3}} (e_1 \otimes e_1 - \frac{1}{2} e_2 \otimes e_2 - \frac{1}{2} e_3 \otimes e_3), & U_5 &:= \frac{1}{\sqrt{2}} (e_2 \otimes e_2 - e_3 \otimes e_3), \end{aligned}$$

and the following orthonormal basis of  $\mathbb{R}_{\text{skew}}^{3 \times 3}$ ,

$$K_1 = \frac{1}{\sqrt{2}} (e_2 \otimes e_3 - e_3 \otimes e_2), \quad K_2 = \frac{1}{\sqrt{2}} (e_1 \otimes e_2 - e_2 \otimes e_1), \quad K_3 = \frac{1}{\sqrt{2}} (e_1 \otimes e_3 - e_3 \otimes e_1).$$

**Lemma 2.9** (Coordinatewise representation).



(a) For  $i = 1, 2, 3$  consider

$$\Psi_i := P_{\mathbb{H}_{\text{macro}}} \left( \text{sym} (K_i \bar{\mathbf{x}} \otimes e_1) \right)$$

and define  $\mathbb{Q} \in \mathbb{R}_{\text{sym}}^{3 \times 3}$  and  $\mathbb{U} \in \mathbb{R}^{3 \times 5}$  as

$$\begin{aligned} \mathbb{Q}_{ij} &:= (\Psi_i, \Psi_j)_Q, & \text{for } i, j = 1, 2, 3, \\ \mathbb{U}_{ij} &:= (\mathbf{1}_{S_0} U_j, \Psi_i)_Q & \text{for } i = 1, 2, 3, j = 1, \dots, 5. \end{aligned}$$

Then for all  $K \in \mathbb{R}_{\text{skew}}^{3 \times 3}$  and  $U \in \mathbb{R}_{\text{dev}}^{3 \times 3}$  we have

$$\bar{Q}(K) = k \cdot \mathbb{Q} k, \quad k := (K \cdot K_1, \dots, K \cdot K_3)^\top, \quad (12)$$

$$K_{\text{pre}}(U) = \sum_{i=1}^3 (\mathbb{Q}^{-1} \mathbb{U} u)_i K_i, \quad u := \frac{1}{2} (U \cdot U_1, \dots, U \cdot U_5)^\top. \quad (13)$$

(b) For  $j = 1, \dots, 5$  consider

$$\Phi_j := \mathbf{1}_{S_0} U_j - P_{\mathbb{H}_{\text{rel}}} (\mathbf{1}_{S_0} U_j) - \sum_{i=1}^3 (\mathbb{Q}^{-1} \mathbb{U})_{ij} \Psi_i,$$

and define  $\mathbb{E}_{\text{res}} \in \mathbb{R}_{\text{sym}}^{5 \times 5}$  as

$$\mathbb{E}_{\text{res}, ij} := (\Phi_i, \Phi_j)_Q, \quad \text{for } i, j = 1, \dots, 5.$$

Then for all  $U \in \mathbb{R}_{\text{dev}}^{3 \times 3}$  we have

$$E_{\text{res}}(U) = u \cdot \mathbb{E}_{\text{res}} u, \quad u := \frac{1}{2} (U \cdot U_1, \dots, U \cdot U_5)^\top. \quad (14)$$

The orthogonal projections onto  $\mathbb{H}_{\text{macro}}$  and  $\mathbb{H}_{\text{rel}}$  appearing in the definition of  $\Psi_i$  and  $\Phi_j$  lead to corrector problems that take the form of quadratic minimization problems whose solutions are characterized by linear elliptic systems:

**Lemma 2.10** (Corrector equations). *For  $i = 1, 2, 3$  and  $j = 1, \dots, 5$ , let  $(a_i, \varphi_i)$  and  $(a_{U_j}, \varphi_{U_j})$  denote the unique minimizer in  $\mathbb{R} \times H_{\text{av}}^1(S; \mathbb{R}^3)$  of the functional*

$$(a, \varphi) \mapsto \int_S Q(\bar{\mathbf{x}}, F + (a e_1, \bar{\nabla} \varphi)) d\bar{\mathbf{x}}, \quad (15)$$

with  $F = \text{sym}(K_i \bar{\mathbf{x}} \otimes e_1)$  and  $F = \mathbf{1}_{S_0} U_j$ , respectively. Then

$$\begin{aligned} \Psi_i &= \text{sym} \left( K_i \bar{\mathbf{x}} \otimes e_1 + (a_i e_1, \bar{\nabla} \varphi_i) \right), \\ \Phi_j &= \mathbf{1}_{S_0} U_j + \text{sym} (a_{U_j}, \bar{\nabla} \varphi_{U_j}) - \sum_{i=1}^3 (\mathbb{Q}^{-1} \mathbb{U})_{ij} \Psi_i. \end{aligned}$$

## 2.4 The special case of an isotropic material with circular cross-section

We consider the special case of a homogeneous, isotropic material, i.e.,

$$Q(G) = \frac{\lambda}{2} (\text{trace } G)^2 + \mu |\text{sym } G|^2. \quad (16)$$

In that case the formulas for  $\bar{Q}$  and  $K_{\text{pre}}$  become more explicit. They further simplify if we consider bi-rods with a circular cross-section:

**Lemma 2.11** (The isotropic case and the case with a circular cross-section). *Let  $\alpha_S \in H^1(S)$  denote the unique minimizer to*

$$\oint_S \left| \begin{pmatrix} \partial_2 \alpha_S \\ \partial_3 \alpha_S \end{pmatrix} + \frac{1}{\sqrt{2}} \begin{pmatrix} x_3 \\ -x_2 \end{pmatrix} \right|^2 d\bar{x} \quad \text{subject to} \quad \int_S \alpha_S d\bar{x} = \int_S \partial_2 \alpha_S d\bar{x} = \int_S \partial_3 \alpha_S d\bar{x} = 0, \quad (17)$$

and set

$$c_S := \oint_S \left| \begin{pmatrix} \partial_2 \alpha_S \\ \partial_3 \alpha_S \end{pmatrix} + \frac{1}{\sqrt{2}} \begin{pmatrix} x_3 \\ -x_2 \end{pmatrix} \right|^2 d\bar{x}.$$

Assume (16). Then:

(a) We have  $\mathbb{Q} = \text{diag}(q_1, q_2, q_3)$  where

$$q_1 := \frac{\mu}{2} c_S, \quad q_2 := \frac{\mu(3\lambda + 2\mu)}{\lambda + \mu} \oint_S \frac{x_2^2}{4} d\bar{x}, \quad q_3 := \frac{\mu(3\lambda + 2\mu)}{\lambda + \mu} \oint_S \frac{x_3^2}{4} d\bar{x},$$

and

$$\begin{aligned} K_{\text{pre}}(U) = & \left( u_2 \left( \frac{\sqrt{2}}{|S|c_S} \int_{S_0} \partial_2 \alpha_S + \frac{x_3}{\sqrt{2}} d\bar{x} \right) + u_3 \left( \frac{\sqrt{2}}{|S|c_S} \int_{S_0} \partial_3 \alpha_S - \frac{x_2}{\sqrt{2}} d\bar{x} \right) \right) K_1 \\ & + u_4 \left( \frac{2}{\sqrt{3}} \frac{\int_{S_0} x_2 d\bar{x}}{\int_S x_2^2 d\bar{x}} \right) K_2 + u_4 \left( \frac{2}{\sqrt{3}} \frac{\int_{S_0} x_3 d\bar{x}}{\int_S x_3^2 d\bar{x}} \right) K_3, \end{aligned}$$

where  $u_1, \dots, u_5$  are defined as in (13).

(b) In the case of a circular cross-section,  $S = B(0; \pi^{-\frac{1}{2}})$ , we have  $\alpha_S = 0$ ,  $c_S = \frac{1}{4\pi}$ , and

$$q_1 = \frac{1}{8\pi} \mu, \quad q_2 = q_3 = \frac{1}{16\pi} \frac{\mu(3\lambda + 2\mu)}{\lambda + \mu}.$$

If in addition  $S_0 = S \cap \{x_3 \geq 0\}$ , then

$$K_{\text{pre}}(U) = \frac{8u_2}{3\sqrt{\pi}} K_1 + \frac{16u_4}{3\sqrt{3\pi}} K_3,$$

where  $u_1, \dots, u_5$  are defined as in (13).

### 3 Simulation and model exploration

For our numerical experiments, we use a discrete gradient flow approach based on the work in [BR20] in order to numerically approximate critical points of the energy functional  $\mathcal{E}$ . For convenience we use the notation  $y', y'', \dots$  to denote derivatives with regard to  $x_1$ . Furthermore, in this section we use  $h$  to denote the discretization scale (and not the thickness of the three-dimensional domain as in the previous section).

We first bring the energy functional  $\mathcal{E}$  into a form that is similar to the one considered in [BR20]. Note that for a framed curve  $(y, R)$  the columns of the rotational frame take the form

$$R = (y', b, y' \wedge b), \quad \text{where } b := Re_2.$$

We may introduce two bending components and a twist rate of the curve via

$$\kappa_b := y'' \cdot b, \quad \kappa_d := y'' \cdot (y' \wedge b) \quad \text{and} \quad \beta := b' \cdot (y' \wedge b),$$

and deduce that

$$K = R^\top \partial_1 R = \begin{pmatrix} 0 & -\kappa_b & -\kappa_d \\ \kappa_b & 0 & \beta \\ \kappa_d & -\beta & 0 \end{pmatrix} = \sqrt{2}(\beta K_1 + \kappa_b K_2 + \kappa_d K_3),$$

where  $K_1, K_2, K_3$  denote the orthonormal basis of  $\mathbb{R}_{\text{skew}}^{3 \times 3}$  introduced above. Motivated by this we introduce the functional

$$\begin{aligned} \bar{\mathcal{E}}(y, b, \hat{n}) &= \frac{1}{2} \int_{\omega} \bar{Q}(K + \bar{r} K_{\text{pre}}(U(\hat{n}))) + \bar{r}^2 E_{\text{res}}(U(\hat{n})) dx_1 \\ &\quad + \frac{1}{2} \kappa^2 \int_{\omega} |(R\hat{n})'|^2 dx_1, \end{aligned}$$

where

$$U(\hat{n}) := \frac{1}{3} \mathbf{I} - \hat{n} \otimes \hat{n}, \quad \hat{n} := R^\top n, \quad R := (y', b, y' \wedge b), \quad (18)$$

and note that we have  $\mathcal{E}(y, R, n) = 2\bar{\mathcal{E}}(y, b, \hat{n})$  provided  $y, R, b, n$  and  $\hat{n}$  are related by (18).

We note that with help of  $\hat{n}$  (which is just the LCE-director  $n$  expressed in local coordinates), the terms  $K_{\text{pre}}(U(\hat{n}))$  and  $E_{\text{res}}(U(\hat{n}))$  become independent of  $y$  and  $R$ —a property that will simplify the form of the gradient of  $\bar{\mathcal{E}}$ .

In the isotropic case, which we shall consider from now on, the expression further simplifies by appealing to Lemma 2.11, and we obtain

$$\begin{aligned} \bar{\mathcal{E}}(y, b, \hat{n}) &= \frac{1}{2} \int_{\omega} \bar{q}_1 |\beta - \bar{r} k_1(U(\hat{n}))|^2 + \bar{q}_2 |\kappa_b - \bar{r} k_2(U(\hat{n}))|^2 \\ &\quad + \bar{q}_3 |\kappa_d - \bar{r} k_3(U(\hat{n}))|^2 + \bar{r}^2 E_{\text{res}}(U(\hat{n})) dx_1 \\ &\quad + \frac{1}{2} \kappa^2 \int_{\omega} |(R\hat{n})'|^2 dx_1, \end{aligned}$$

where for  $i = 1, 2, 3$ , the linear maps  $k_i : \mathbb{R}_{\text{dev}}^{3 \times 3} \rightarrow \mathbb{R}$  are given by  $k_i(U) = \frac{1}{\sqrt{2}} K_{\text{pre}}(U) \cdot K_i$ . By appealing to binomial formulas and the relations  $|y''|^2 = |\kappa_b|^2 + |\kappa_d|^2$  and  $|b'|^2 = |\kappa_b|^2 + |\beta|^2$ , we eventually get

$$\begin{aligned} \bar{\mathcal{E}}(y, b, \hat{n}) &= \frac{1}{2} \int_{\omega} \bar{q}_3 |y''|^2 + \bar{q}_1 |b'|^2 + \kappa^2 |(R\hat{n})'|^2 dx_1 \\ &\quad + G(y, b) + \bar{\mathcal{E}}_{\text{res}}(\hat{n}) + N(y, b, \hat{n}) \end{aligned} \quad (19)$$

with the functionals

$$\begin{aligned} G(y, b) &= \frac{1}{2} (\bar{q}_2 - \bar{q}_1 - \bar{q}_3) \int_{\omega} |y'' \cdot b|^2 dx_1, \\ \bar{\mathcal{E}}_{\text{res}}(\hat{n}) &= \frac{1}{2} \bar{r}^2 \int_{\omega} E_{\text{res}}(U(\hat{n})) dx_1 \quad \text{and} \\ N(y, b, \hat{n}) &= \int_{\omega} \frac{1}{2} \bar{r}^2 \sum_{i=1}^3 \bar{q}_i |k_i(U(\hat{n}))|^2 - \bar{r} \bar{q}_1 (b' \cdot (y' \wedge b)) k_1(U(\hat{n})) \\ &\quad - \bar{r} \bar{q}_2 (y'' \cdot b) k_2(U(\hat{n})) - \bar{r} \bar{q}_3 (y'' \cdot (y' \wedge b)) k_3(U(\hat{n})) dx_1. \end{aligned}$$

The structure of the energy functional (19) is similar to the bending-twisting energy that was used in [BR20] with the difference that we now have additional terms which depend on the LCE-director  $\hat{n}$ .

### 3.1 Numerical minimization by a discrete gradient flow

Next, we introduce a suitable discretisation. For the approximation of the deformation  $y$ , our approach uses piecewise cubic,  $C^1$ -conforming elements, whereas the frame director  $b$  and the LCE-director  $\hat{n}$  are approximated via piecewise linear, continuous elements. More specifically, following [Bar20] we consider a partitioning of  $\bar{\omega} = [0, L]$  defined by sets of nodes  $\mathcal{N}_h$  and elements  $\mathcal{T}_h$ , and denote by

$$\begin{aligned}\mathcal{S}^{1,0}(\mathcal{T}_h) &= \{b_h \in C^0(\bar{\omega})\} : b_h|_T \in P_1(T) \text{ for all } T \in \mathcal{T}_h, \\ \mathcal{S}^{3,1}(\mathcal{T}_h) &= \{y_h \in C^1(\bar{\omega})\} : y_h|_T \in P_3(T) \text{ for all } T \in \mathcal{T}_h,\end{aligned}$$

the associated spaces of piecewise linear and continuous (resp. piecewise cubic and  $C^1$ -conforming) finite elements. Moreover, we introduce the discrete space

$$V_{\text{LCE}}^h = \mathcal{S}^{3,1}(\mathcal{T}_h)^3 \times \mathcal{S}^{1,0}(\mathcal{T}_h)^3 \times \mathcal{S}^{1,0}(\mathcal{T}_h)^3.$$

On this vector space we define a discrete energy functional  $\bar{\mathcal{E}}_{h,\varepsilon}$ , which contains the same terms as  $\bar{\mathcal{E}}$ —in some cases with appropriate quadrature—as well as a penalty term to approximately incorporate the constraint  $y' \cdot b = 0$ : For  $(y_h, b_h, \hat{n}_h) \in V_{\text{LCE}}^h$  let  $R_h = (y_h', b_h, y_h' \wedge b_h)$  and define

$$\begin{aligned}\bar{\mathcal{E}}_{h,\varepsilon}(y_h, b_h, \hat{n}_h) &= \frac{1}{2} \int_{\omega} \bar{q}_3 |y_h''|^2 + \bar{q}_1 |b_h'|^2 + \kappa^2 |(R_h \hat{n}_h)'|^2 dx_1 \\ &\quad + P_{h,\varepsilon}(y_h, b_h) + G_h(y_h, b_h) + \bar{\mathcal{E}}_{\text{res},h}(\hat{n}_h) + N_h(y_h, b_h, \hat{n}_h),\end{aligned}\tag{20}$$

where the aforementioned penalty term is defined as

$$P_{h,\varepsilon}(y_h, b_h) = \frac{1}{2\varepsilon} \int_{\omega} \mathcal{I}_h^{1,0}[(y_h' \cdot b_h)^2] dx_1.$$

Above,  $\mathcal{I}_h^{1,0}$  denotes the nodal interpolation operator associated with  $\mathcal{S}^{1,0}(\mathcal{T}_h)$  and  $\varepsilon > 0$  a parameter to adjust the penalization. The functionals  $G_h$ ,  $\bar{\mathcal{E}}_{\text{res},h}$  and  $N_h$  are discrete versions of  $G$ ,  $\bar{\mathcal{E}}_{\text{res}}$  and  $N$  respectively, that contain nodal interpolation operators on the related discrete spaces to simplify the computation of the integrals.

The energy (20) is minimized in the discretized admissible set

$$\begin{aligned}\mathcal{A}_h &:= \{(y_h, b_h, \hat{n}_h) \in V_{\text{LCE}}^h : L_{\text{BC}}(y_h, b_h, \hat{n}_h) = \ell_{\text{BC}}, \\ &\quad |y_h'(z)| = |b_h(z)| = |\hat{n}(z)| = 1 \text{ f.a. } z \in \mathcal{N}_h\},\end{aligned}$$

where  $\mathcal{N}_h$  denotes the set of vertices related to  $\mathcal{T}_h$ . The expression  $L_{\text{BC}}(y_h, b_h, \hat{n}_h) = \ell_{\text{BC}}$  implies that  $(y_h, b_h, \hat{n}_h)$  fulfil the boundary conditions specified by  $\ell_{\text{BC}}$ . Different conditions such as fixed, clamped, free and periodic are possible. The boundary conditions for the individual variables are denoted by  $L_{\text{BC},y}$ ,  $L_{\text{BC},b}$  and  $L_{\text{BC},\hat{n}}$ .

We employ a discrete gradient flow scheme to approximate minimizers of the discretized energy and incorporate linearized versions of the unit-length and boundary conditions by restricting each step of the iteration to a corresponding tangent space of the admissible set. For  $(y_h, b_h, \hat{n}_h) \in \mathcal{A}_h$ , these tangent spaces are given by

$$\begin{aligned}\mathcal{F}_{h,y}(y_h) &= \{\delta y_h \in \mathcal{S}^{3,1}(\mathcal{T}_h)^3 : L_{\text{BC},y}(\delta y_h) = 0, y_h'(z) \cdot \delta y_h'(z) = 0 \text{ f.a. } z \in \mathcal{N}_h\}, \\ \mathcal{F}_{h,b}(b_h) &= \{\delta b_h \in \mathcal{S}^{1,0}(\mathcal{T}_h)^3 : L_{\text{BC},b}(\delta b_h) = 0, b_h(z) \cdot \delta b_h(z) = 0 \text{ f.a. } z \in \mathcal{N}_h\}\end{aligned}$$

as well as

$$\mathcal{F}_{h,\hat{n}}(\hat{n}_h) = \{\delta \hat{n}_h \in \mathcal{S}^{1,0}(\mathcal{T}_h)^3 : L_{\text{BC},\hat{n}}(\delta \hat{n}_h) = 0, \hat{n}_h(z) \cdot \delta \hat{n}_h(z) = 0 \text{ f.a. } z \in \mathcal{N}_h\}.$$

Note that the functions in these tangent spaces are required to satisfy homogeneous versions of the given boundary conditions.

The variations of the energy with respect to the different variables are approximated semi-implicitly, where the convex quadratic terms are mostly handled implicitly while we rely on an explicit treatment of the nonlinear and non-convex parts. We let  $(\cdot, \cdot)_Y$ ,  $(\cdot, \cdot)_X$  and  $(\cdot, \cdot)_Z$  denote bilinear forms on the spaces  $\mathcal{S}^{3,1}(\mathcal{T}_h)^3$ ,  $\mathcal{S}^{1,0}(\mathcal{T}_h)^3$  and  $\mathcal{S}^{1,0}(\mathcal{T}_h)^3$  respectively and use the backwards difference quotient  $d_t$ .

**Algorithm 3.1.** Set initial values  $(y_h^0, b_h^0, \hat{n}_h^0) \in \mathcal{A}_h$ , a timestep size  $\tau$ , a stopping criterion  $\varepsilon_{\text{stop}}$  and initialize  $k = 1$ .

(1) Compute  $y_h^k = y_h^{k-1} + \tau d_t y_h^k$  with  $d_t y_h^k \in \mathcal{F}_{h,y}(y_h^{k-1})$  such that

$$\begin{aligned} & \left( d_t y_h^k, \delta y_h \right)_Y + \bar{q}_3 \left( [y_h^k]'', \delta y_h'' \right)_{L^2(\omega)} + \frac{\partial P_{h,\varepsilon}(y_h^k, b_h^{k-1})}{\partial y_h^k} [\delta y_h] \\ &= -\kappa^2 \left( \left( \frac{\partial R_h^{k-1}}{\partial y_h^{k-1}} [\delta y_h] \right) \hat{n}_h^{k-1} \right)', (R_h^{k-1} \hat{n}_h^{k-1})' \Big)_{L^2(\omega)} \\ & \quad - \frac{\partial G_h(y_h^{k-1}, b_h^{k-1})}{\partial y_h^{k-1}} [\delta y_h] - \frac{\partial N_h(y_h^{k-1}, b_h^{k-1}, \hat{n}_h^{k-1})}{\partial y_h^{k-1}} [\delta y_h] \end{aligned}$$

for all  $\delta y_h \in \mathcal{F}_{h,y}(y_h^{k-1})$ .

(2) Compute  $b_h^k = b_h^{k-1} + \tau d_t b_h^k$  with  $d_t b_h^k \in \mathcal{F}_{h,b}(b_h^{k-1})$  such that

$$\begin{aligned} & \left( d_t b_h^k, \delta b_h \right)_X + \bar{q}_1 \left( [b_h^k]', \delta b_h' \right)_{L^2(\omega)} + \frac{\partial P_{h,\varepsilon}(y_h^k, b_h^k)}{\partial b_h^k} [\delta b_h] \\ &= -\kappa^2 \left( \left( \frac{\partial R_h^{k-1}}{\partial b_h^{k-1}} [\delta b_h] \right) \hat{n}_h^{k-1} \right)', (R_h^{k-1} \hat{n}_h^{k-1})' \Big)_{L^2(\omega)} \\ & \quad - \frac{\partial G_h(y_h^k, b_h^{k-1})}{\partial b_h^{k-1}} [\delta b_h] - \frac{\partial N_h(y_h^k, b_h^{k-1}, \hat{n}_h^{k-1})}{\partial b_h^{k-1}} [\delta b_h] \end{aligned}$$

for all  $\delta b_h \in \mathcal{F}_{h,b}(b_h^{k-1})$ .

(3) Compute  $\hat{n}_h^k = \hat{n}_h^{k-1} + \tau d_t \hat{n}_h^k$  with  $d_t \hat{n}_h^k \in \mathcal{F}_{h,\hat{n}}(\hat{n}_h^{k-1})$  such that

$$\begin{aligned} & \left( d_t \hat{n}_h^k, \delta \hat{n}_h \right)_Z + \kappa^2 \left( (R_h^k \hat{n}_h^k)', (R_h^k \delta \hat{n}_h)' \right)_{L^2(\omega)} \\ &= - \frac{\partial \bar{\mathcal{E}}_{\text{res},h}(\hat{n}_h^{k-1})}{\partial \hat{n}_h^{k-1}} [\delta \hat{n}_h] - \frac{\partial N_h(y_h^k, b_h^k, \hat{n}_h^{k-1})}{\partial \hat{n}_h^{k-1}} [\delta \hat{n}_h] \end{aligned}$$

for all  $\delta \hat{n}_h \in \mathcal{F}_{h,\hat{n}}(\hat{n}_h^{k-1})$ .

(4) Stop the iteration if  $\|d_t y_h^k\|_Y + \|d_t b_h^k\|_X + \|d_t \hat{n}_h^k\|_Z \leq \varepsilon_{\text{stop}}$ . Otherwise set  $k \mapsto k + 1$  and continue with (1).

### 3.2 Numerical experiments

The experiments we present serve the purpose of investigating properties of the LCE-model and the proposed algorithm. Stability and convergence can be investigated following the scheme

presented in [BR20], where these results are available. Additionally, our experiments indicate stability, at least for the parameters specified below.

We simulate an elastic rod made of a nearly incompressible isotropic material by using the Lamé parameters  $\lambda = 1000$  and  $\mu = 1$  and assume it to have a circular cross-section where the LCE-material fills one semi-circle, i.e.

$$S = B(0; \pi^{-\frac{1}{2}}), \quad S_0 = S \cap \{\bar{x} = (x_2, x_3) : x_3 > 0\}.$$

With these specifications and Lemma 2.11, we are able to infer the representations of  $\bar{Q}$  and  $K_{\text{pre}}$ . For  $E_{\text{res}}$ , the Lemmas 2.9 and 2.10 imply that we need to solve several quadratic minimization problems to assemble the matrix  $\mathbb{E}_{\text{res}}$ . The corresponding linear elliptic systems are approximately solved using a standard finite-element-method and lead to

$$\mathbb{E}_{\text{res}} = 10^{-2} \begin{pmatrix} 0.95 & 0 & 0 & 0 & 0 \\ 0 & 10.77 & -0.01 & 0 & 0 \\ 0 & -0.01 & 0.18 & 0 & 0 \\ 0 & 0 & 0 & 34.94 & 0 \\ 0 & 0 & 0 & 0 & 4.9 \end{pmatrix}.$$

This matrix characterizes  $E_{\text{res}}$  with regard to the basis  $\{U_1, \dots, U_5\}$  of  $\mathbb{R}_{\text{dev}}^{3 \times 3}$  which is used in Lemma 2.9.

Additionally, we choose the spacial step size  $h = 1/200$  and the constant timestep size  $\tau = h/2 = 1/400$  as well as the model parameter  $\varepsilon = 1/200$ . For  $y_h, \bar{y}_h \in \mathcal{S}^{3,1}(\mathcal{T}_h)^3$  and  $b_h, \bar{b}_h \in \mathcal{S}^{1,0}(\mathcal{T}_h)^3$ , the bilinear forms we use are given by

$$\begin{aligned} (y_h, \bar{y}_h)_Y &= (y_h, \bar{y}_h)_{L^2(\omega)} + h(y_h'', \bar{y}_h'')_{L^2(\omega)}, \\ (b_h, \bar{b}_h)_X &= (b_h, \bar{b}_h)_Z = (b_h, \bar{b}_h)_{L^2(\omega)} + h(b_h', \bar{b}_h')_{L^2(\omega)}. \end{aligned}$$

We next specify boundary conditions and external forces which we use in our experiments.

**Example 3.1** (Bending via magnetic field). Our first experiment focuses on a straight line from the clamped end  $(0, 0, 0)$  to the free end  $(2, 0, 0)$ . In the beginning  $y' = (1, 0, 0)$ ,  $b = (0, 1, 0)$ ,  $d = (0, 0, 1)$  and  $n = \hat{n} = (0, 1, 0)$  are constant. For a visualisation of the starting configurations, see the first graphic in Figure 1.

To simulate a homogeneous magnetic field that forces the LCE-director  $n$  to align with a vector  $f \in \mathbb{R}^3$ , we add the forcing term  $-(f, R\hat{n})_{L^2(\omega)}$  to the energy. The computations of  $y$ ,  $b$  and  $\hat{n}$  are modified accordingly. We split the (quasi-) time interval  $[0, T]$  with  $T = 60$  into the smaller intervals  $I_m = (10(m-1), 10m]$  for  $m = 1, \dots, 6$ . Since we are interested in the LCE-director's influence on bending behaviour, we choose the external field to change periodically between two constant states given by  $f_{\text{odd}} = (0, 1, 0)$  and  $f_{\text{even}} = (1, 0, 0)$ . For  $t \in (0, T)$  and  $x_1 \in \omega$  we thus define

$$f(t, x_1) := \begin{cases} f_{\text{odd}} & \text{if } t \in I_m, m \text{ is odd,} \\ f_{\text{even}} & \text{if } t \in I_m, m \text{ is even.} \end{cases}$$

The remaining parameters we use are  $\bar{r} = \kappa = 1$ .

In the Figures 2 and 3 we can see the development of energy and deformation within  $(0, T)$ . For both values of  $f$  we observe a different deformation the rod seems to converge to, basically enabling us to switch between two states. However, the deformations and energy at the end of the different time intervals corresponding to the same value of  $f$  are slightly different. This can be explained by the fact, that these intervals are too short for a full relaxation and convergence to the minimizer. Indeed we observe smaller differences when using longer time intervals.

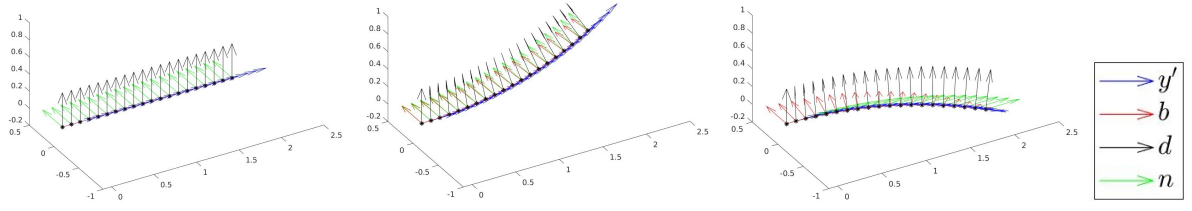


Figure 1: Deformation of the rod in Example 3.1. From left to right we have  $t = 0$ ,  $t = 30$  and  $t = 40$ . The different coloured arrows represent the vectors  $y'$ ,  $b$  and  $d = y' \wedge b$ , that form the frame  $R$ , as well as the LCE-director  $n = R\hat{n}$ . The two rightmost graphics show, that the LCE-director  $n$  tends to align with the vectors  $f_{\text{odd}} = (0, 1, 0)$  or  $f_{\text{even}} = (1, 0, 0)$  at the end of the intervals  $I_3$  and  $I_4$  respectively.

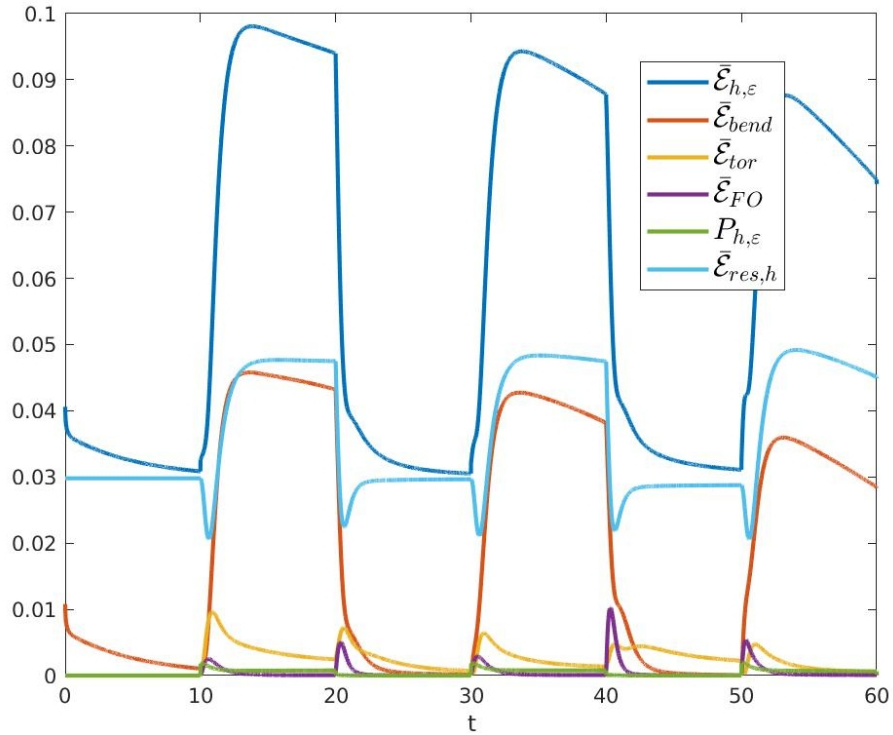


Figure 2: Energy development over the (quasi-) time interval in Example 3.1. The different curves represent the energy term  $\bar{\mathcal{E}}_{h,\varepsilon}$ , the bending energy, the torsion energy, the Frank-Oseen energy, the penalty term  $P_{h,\varepsilon}$  and the contribution of  $\bar{\mathcal{E}}_{\text{res},h}$ . The energy is non-decreasing in some parts. This is due to the fact that the energy functional  $\bar{\mathcal{E}}_{h,\varepsilon}$  does not include the forcing term  $-(f, R\hat{n})_{L^2(\omega)}$ , which was added to simulate a magnetic field, and it takes some time until  $n$  and  $f$  are realigned after  $f$  changes.

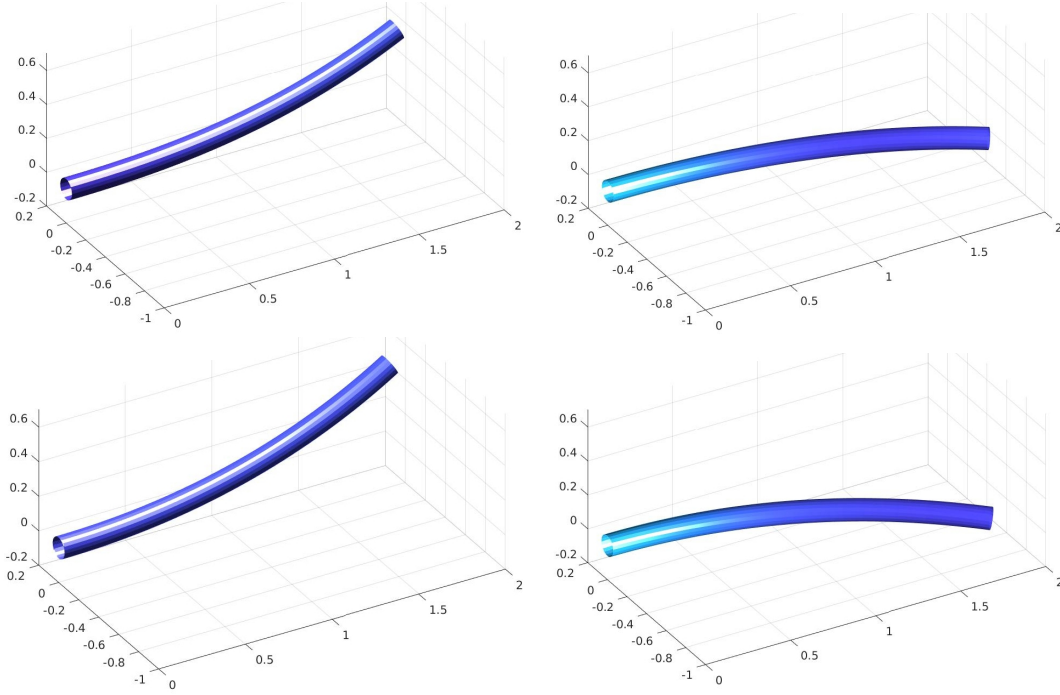


Figure 3: Deformation of the rod from Example 3.1. The top row shows the configurations at  $t = 10$  and  $t = 20$ , while the bottom row shows  $t = 30$  and  $t = 40$ . The colouring of the tube represents its curvature.

**Example 3.2** (Buckling). In our second experiment, we aim to investigate the buckling behaviour of an LCE-rod. Again, we have a straight line from  $(0,0,0)$  to  $(2,0,0)$ . This time however, both ends are clamped and the rod is twisted twice. The initial LCE-director is  $n = R\hat{n} = b$ . This configuration can be seen in the first graphic of Figure 4.

In order to induce buckling behaviour, we modify the boundary conditions to move the end at  $(2,0,0)$  towards  $(0,0,0)$  with a velocity of  $(-1,0,0)$ . At  $t = 1$ , when the end on the right-hand side is located at  $(1,0,0)$ , we stop this movement and let the rod relax until  $T = 50$ . Since we are interested in the influence of the parameter  $\bar{r}$ , we fix  $\kappa = 0.4$  and carry out the experiment for  $r = 1, \dots, 10$ .

Figures 4 and 5 show the deformation at the end of the time frame for various values of  $\bar{r}$ . We observe a significant difference between the choice  $\bar{r} = 1$  and the other cases. In order to understand the dependence, we take a look at the energy plots which can be seen in Figure 6. The cases  $\bar{r} = 1$  and  $\bar{r} = 2$  have a steep decline of mostly the torsion energy at some point after the curve initially flattens. In the other cases, this decline is not present within the given time frame. (Indeed, even when choosing a significantly longer time frame, the decline does not happen for  $\bar{r} \geq 3$ .)

The reason for the aforementioned decline is shown in Figure 7. The rod reaches a more beneficial energetic state by effectively folding over. In doing so, it intersects itself, which is possible due to the lack of a self-avoidance term in our model, but not concerning when we are just interested in minimizing the energy. In reality, the rod would likely be stopped by itself and form a loop, but the behavioural differences based on the parameter  $\bar{r}$  would still be significant. In these two examples, we have seen that the competing contributions of the different energy terms in the LCE rod model result in non-trivial deformations. Additionally, the LCE material has a significant impact on the configuration that minimizes the energy. On the one hand, we



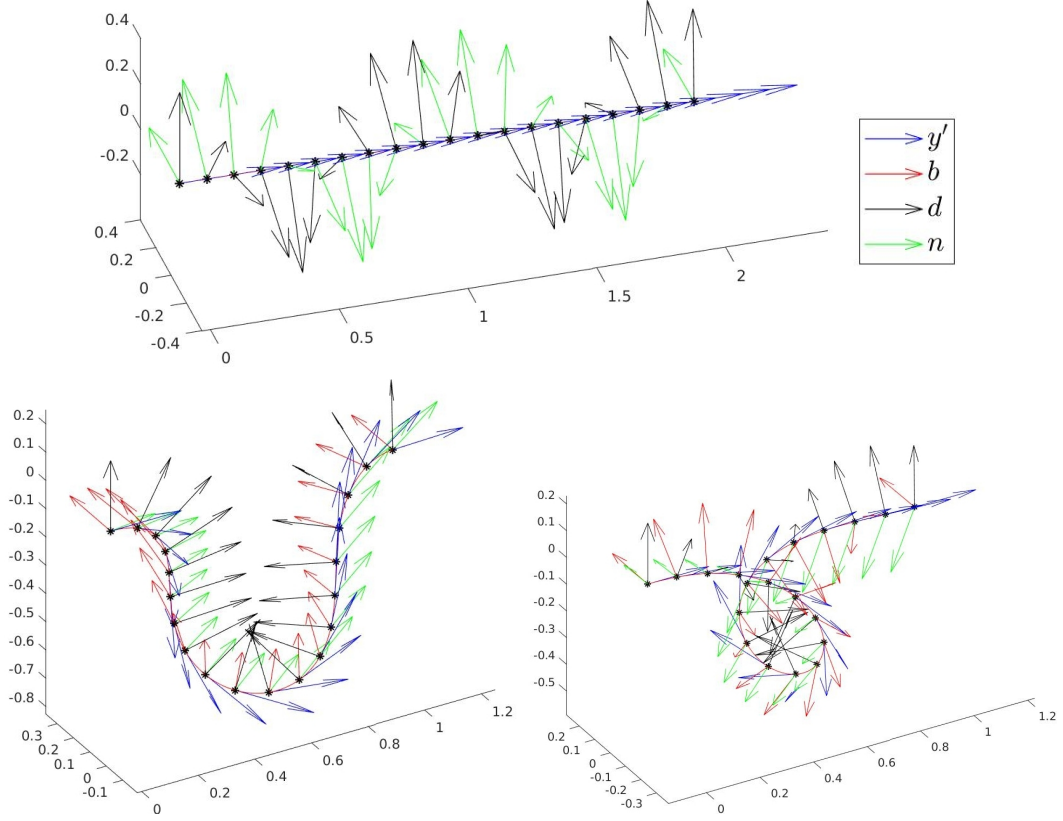


Figure 4: Buckling behaviour of the rod from Example 3.2. The top row shows the starting configuration while the bottom row depicts the relaxed state at time  $t = 50$  with  $\bar{r} = 1$  (left) and  $\bar{r} = 3$  (right). As in Figure 1, the vectors  $y'$ ,  $b$  and  $d = y' \wedge b$ , that form the frame  $R$ , as well as the LCE-director  $n = R\hat{n}$  are shown.

are able to change the bending behaviour of a rod by directly influencing the LCE-director via a simulated magnetic field. On the other hand, we see a change in buckling behaviour when the model parameter  $\bar{r}$  is modified. In practice, this could be realized by altering the surrounding temperature.

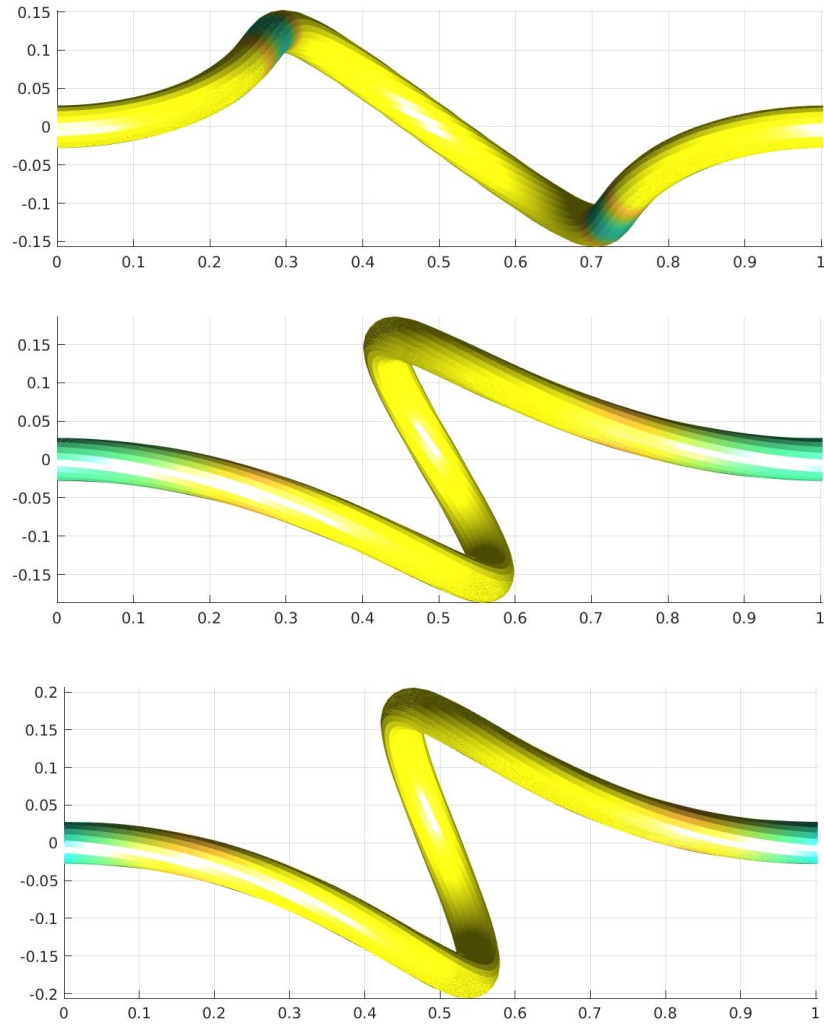


Figure 5: Buckling of the LCE-rod in Experiment 3.2 with  $\bar{r} = 1, 3, 5$  (top to bottom). The line of view is parallel to the  $x_3$ -axis and the colouring of the tube represents its curvature.

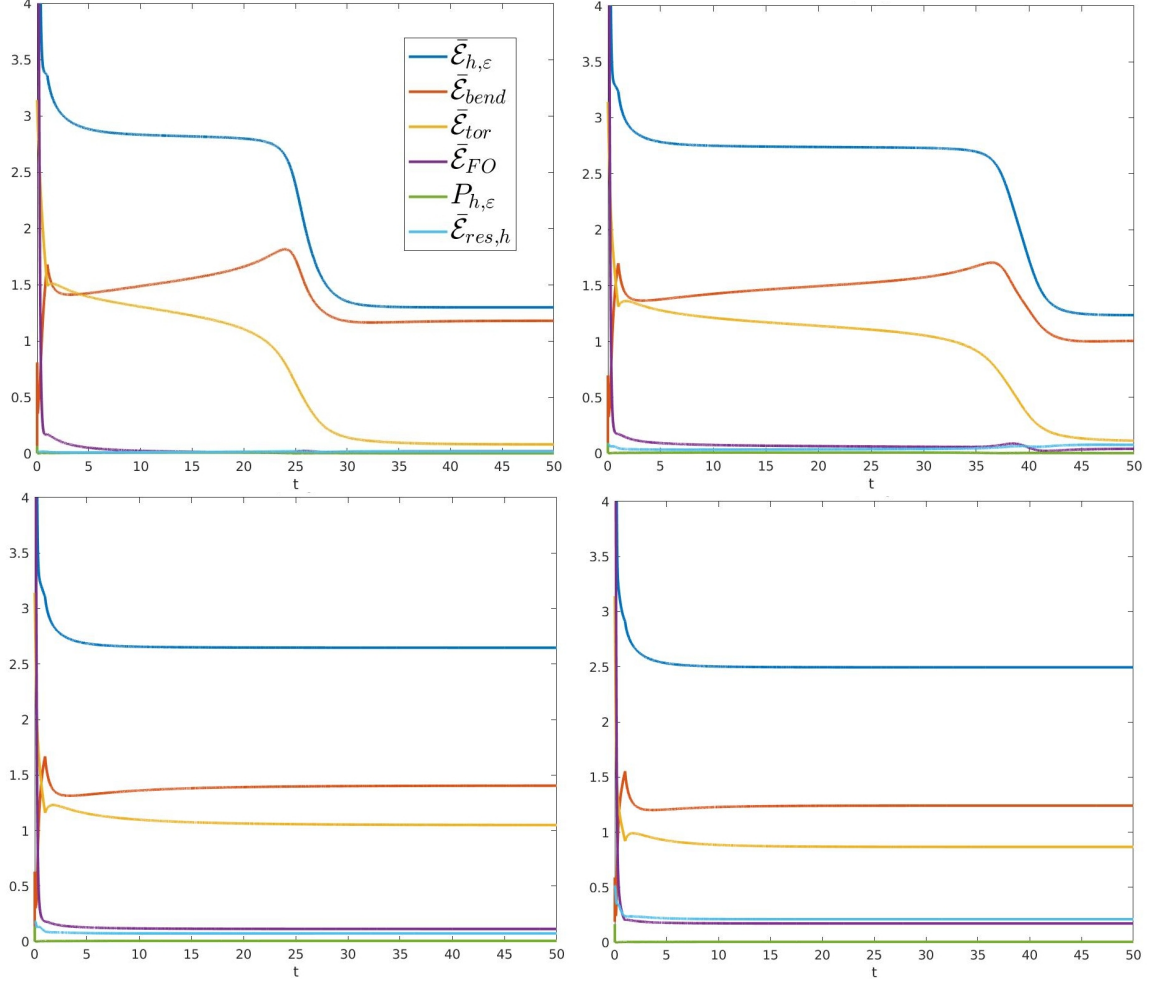


Figure 6: Energy development in Example 3.2. The top row shows the experiments with  $\bar{r} = 1$  and  $\bar{r} = 2$ , while the bottom row shows  $\bar{r} = 3$  and  $\bar{r} = 5$ . Again we see the total energy  $\bar{\mathcal{E}}_{h,\varepsilon}$ , the bending energy, the torsion energy, the Frank-Oseen energy, the penalty term  $P_{h,\varepsilon}$  and the contribution of  $\bar{\mathcal{E}}_{res,h}$ .

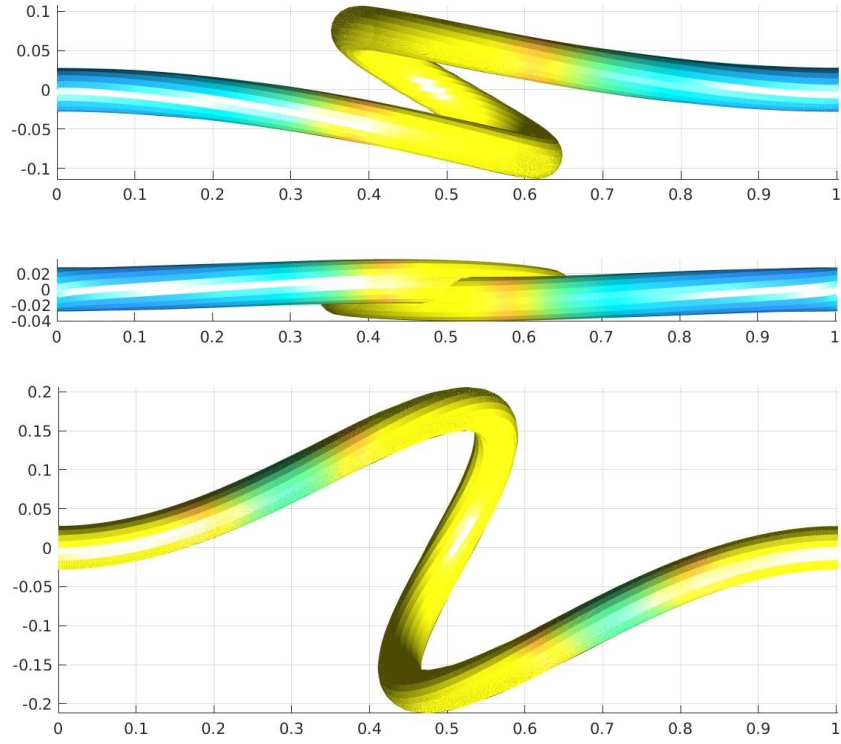


Figure 7: Buckling behaviour of the LCE-rod from Example 3.2. We have  $\bar{r} = 1$  and see the configurations at  $t = 22, 24, 26$  (top to bottom). The rod intersects itself to reach a more beneficial energetic state.

## 4 Proofs

### 4.1 Compactness – Proof of Theorem 2.1 (a) and Proposition 2.2 (a)

In this step we prove (7), (8). Furthermore, we show that there exists  $R_h : \Omega \rightarrow \text{SO}(3)$  and a corrector  $\chi \in L^2(\omega; \mathbb{H}_{\text{rel}})$  such that (for a subsequence) we have

$$\frac{R_h^\top L_h(n_h)^{-\frac{1}{2}} \nabla_h y_h - I}{h} \rightharpoonup \text{sym} \left( (R^\top \partial_1 R \bar{x}) \otimes e_1 \right) + \frac{\bar{r}}{2} \chi_{\Omega_0} R^\top \left( \frac{1}{3} I - n \otimes n \right) R + \chi. \quad (21)$$

Indeed, by the argument of [BGN<sup>+</sup>22, Lemma 4.1] we see that  $\limsup_{h \rightarrow 0} \mathcal{E}_h(y_h, n_h) < \infty$  implies

$$\limsup_{h \rightarrow 0} \frac{1}{h^2} \int_{\Omega} \text{dist}^2(\nabla_h y_h, \text{SO}(3)) < \infty, \quad (22)$$

$$\limsup_{h \rightarrow 0} \int_{\Omega} |\nabla_h y_h|^q + |\det(\nabla_h y_h)|^{-\frac{q}{2}} < \infty, \quad (23)$$

$$\limsup_{h \rightarrow 0} \int_{\Omega_0} |\nabla_h n_h (\nabla_h y_h)^{-1}|^2 |\det(\nabla_h y_h)| < \infty, \quad (24)$$

$$\limsup_{h \rightarrow 0} \int_{\Omega_0} |\nabla_h n_h|^p < \infty, \quad \text{where } p = \frac{2q}{q+4}, \quad (25)$$

and we find  $\bar{h} > 0$  (depending on the sequence) such that

$$\det(\nabla_h y_h) > 0 \text{ a.e. in } \Omega \quad \text{for all } 0 < h \leq \bar{h}. \quad (26)$$

From now on we assume that  $0 < h \leq \bar{h}$ .

Thanks to (25) we find  $n \in H^1(\omega; \mathbb{S}^2)$  such that (up to a subsequence) we have  $n_h \rightharpoonup n$  weakly in  $W^{1,p}(\Omega_0)$  and pointwise a.e. in  $\Omega_0$ . Since  $(n_h)$  is bounded in  $L^\infty$ , (8) follows. Furthermore, by appealing to [BNS20, Proposition 5.1 (a)] we conclude that there exists a subsequence (not relabeled), and a rod configuration  $(y, R)$  such that (7) holds and

$$E_h(y_h) \rightharpoonup E := \text{sym} \left( (R^\top \partial_1 R \bar{x}) \otimes e_1 \right) + \chi \quad \text{weakly in } L^2, \quad (27)$$

for a corrector  $\chi \in L^2(\omega; \mathbf{H}_{\text{rel}})$ . To prove (21) we proceed as follows: In view of (26) and thanks to the polar decomposition we find  $R_h : \Omega \rightarrow \text{SO}(3)$  such that

$$\nabla_h y_h(x) = R_h(x) \sqrt{\nabla_h y_h(x)^\top \nabla_h y_h(x)}.$$

We set  $G_h := \frac{R_h^\top \nabla_h y_h - I}{h}$  and note that (27) implies  $G_h \rightharpoonup E$  weakly in  $L^2$  and  $R_h \rightarrow R$  strongly in  $L^2$ . Next, we rewrite the elastic part of the strain as follows,

$$\left( I + \chi_{\Omega_0} (L_h(n_h)^{-\frac{1}{2}} - I) \right) \nabla_h y_h = R_h (I + h \tilde{B}_h) (I + h G_h), \quad \tilde{B}_h := \chi_{\Omega_0} R_h^\top \left( \frac{L_h(n_h)^{-\frac{1}{2}} - I}{h} \right) R_h.$$

In view of the construction of  $L_h^{-\frac{1}{2}}$ , the boundedness of  $n_h$ , and the pointwise convergence of  $n_h$  and  $R_h$  a.e. in  $\Omega_0$ , we deduce that  $(\tilde{B}_h)$  is bounded in  $L^\infty(\Omega)$ , and

$$\tilde{B}_h \rightarrow \frac{\bar{r}}{2} \chi_{\Omega_0} R^\top \left( \frac{1}{3} I - n \otimes n \right) R \quad \text{in } L^2(\Omega).$$

In combination with  $G_h \rightharpoonup E$ , (21) follows.  $\square$

## 4.2 Lower bound – Proof of Theorem 2.1 (b)

By passing to a subsequence (not relabeled) and by appealing to compactness in form of Theorem 2.1 (a), we may assume without loss of generality that (21) holds, and

$$\liminf_{h \rightarrow 0} \mathcal{E}_h(y_h, n_h) = \lim_{h \rightarrow 0} \mathcal{E}_h(y_h, n_h) < \infty.$$

From (21) we infer with the argument of [BGN<sup>+</sup>22, Proof of Theorem 2.3(b)] that

$$\begin{aligned} & \liminf_{h \rightarrow 0} \frac{1}{h^2 |S|} \left( \int_{\Omega \setminus \Omega_0} W(\nabla_h y_h(x)) dx + \int_{\Omega_0} W(L_h(n_h(x))^{-\frac{1}{2}} \nabla_h y_h(x)) dx \right) \\ & \geq \frac{1}{|S|} \int_{\Omega} Q \left( \text{sym} \left( (R^\top \partial_1 R \bar{x}) \otimes e_1 \right) + \frac{\bar{r}}{2} \chi_{\Omega_0} R^\top \left( \frac{1}{3} I - n \otimes n \right) R + \chi \right) dx \\ & \geq \int_{\omega} \min_{\chi \in \mathbb{H}_{\text{rel}}} \int_S Q \left( \text{sym} \left( (R^\top \partial_1 R \bar{x}) \otimes e_1 \right) + \frac{\bar{r}}{2} \chi_{S_0} R^\top \left( \frac{1}{3} I - n \otimes n \right) R + \chi \right) d\bar{x} dx_1. \end{aligned}$$

We combine this with Lemma 2.7 to deduce

$$\begin{aligned} & \liminf_{h \rightarrow 0} \frac{1}{h^2 |S|} \left( \int_{\Omega \setminus \Omega_0} W(\nabla_h y_h(x)) dx + \int_{\Omega_0} W(L_h(n_h(x))^{-\frac{1}{2}} \nabla_h y_h(x)) dx \right) \\ & \geq \int_{\omega} \bar{Q} \left( R^\top \partial_1 R + \bar{r} K_{\text{pre}} \left( \frac{1}{3} I - R^\top n \otimes R^\top n \right) \right) + \bar{r}^2 E_{\text{res}} \left( \frac{1}{3} I - R^\top n \otimes R^\top n \right) dx_1. \end{aligned} \quad (28)$$

It remains to treat the Frank-Oseen energy. By (7) and (8) we have  $(\nabla_h y_h, n_h) \rightarrow (R, n)$  in  $L^2$ . Furthermore, by the a priori bound (25) we have (up to a subsequence and for some  $p \in (1, 2)$ )  $\nabla_h n_h \rightarrow (\partial_1 n, d)$  in  $L^p$  where  $d \in L^p(\Omega_0; \mathbb{R}^{3 \times 2})$ . As in the proof of [BGN<sup>+</sup>22, Theorem 2.3 (a)] we conclude that  $\nabla_h n_h \nabla_h y_h^{-1} (\det \nabla_h y_h)^{\frac{1}{2}} \rightharpoonup (\partial_1 n, d) R^\top$  weakly in  $L^p$ , and thus, by lower semicontinuity, we get

$$\begin{aligned} \liminf_{h \rightarrow 0} \frac{1}{|S_0|} \int_{\Omega_0} |\nabla_h n_h \nabla_h y_h^{-1}|^2 \det \nabla_h y_h dx & \geq \int_{\omega} \int_{S_0} |(\partial_1 n, d) R^\top|^2 d\bar{x} dx_1 \\ & \geq \int_{\omega} |\partial_1 n|^2 dx_1, \end{aligned}$$

where for the last step we used  $|(\partial_1 n, d) R^\top|^2 = |(\partial_1 n, d)|^2 \geq |\partial_1 n|^2$ . In combination with (28) the claimed lower bound follows.  $\square$

## 4.3 Upper bound – Proofs of Theorem 2.1 (c) and Proposition 2.2 (b)

The statements of Theorem 2.1 (c) and Proposition 2.2 (b) directly follow from the following stronger statement (which we shall also use in the proof of Proposition 2.3): For all  $(y, R, n) \in \mathcal{A}$  and  $\beta \in [0, 1)$  there exists a sequence  $(y_h) \subset C^\infty(\bar{\Omega}; \mathbb{R}^3)$  and  $n_h \in H^1(\Omega_0; \mathbb{S}^2)$  such that

$$y_h(0, \bar{x}) = y(0) + h R(0) \bar{x}, \quad (29)$$

and

$$\begin{aligned} \limsup_{h \rightarrow 0} \left( \left| \mathcal{E}(y, R, n) - \mathcal{E}_h(y_h, n_h) \right| + \|y_h - y\|_{L^2} + \|n_h - n\|_{H^1} \right. \\ \left. + h^{-\beta} \|\nabla_h y_h - R\|_{L^\infty} + h^{-\beta} \left\| \frac{(\nabla_h y_h)^\top n_h}{|(\nabla_h y_h)^\top n_h|} - R^\top n \right\|_{L^\infty} \right) = 0. \end{aligned} \quad (30)$$

For the proof we proceed in two steps.

**Step 1.** (Approximation argument).

We first argue that for each  $k \in \mathbb{N}$  we can choose  $(y^k, R^k, n^k) \in \mathcal{A}$  such that  $y^k, R^k \in C^\infty(\bar{\omega})$ ,

$$y^k(0) = y(0), \quad R^k(0) = R(0), \quad (R^k)^\top n^k = R^\top n, \quad (31)$$

and

$$\left| \mathcal{E}(y, R, n) - \mathcal{E}(y^k, R^k, n^k) \right| + \|y - y^k\|_{H^2} + \|R - R^k\|_{L^\infty} + \|\partial_1 R - \partial_1 R^k\|_{L^2} + \|n - n^k\|_{H^1} < \frac{1}{k}. \quad (32)$$

Indeed, in view of the approximation result [Neu12, Lemma 2.3] for all  $\delta > 0$  there exists a smooth framed curve  $(y^k, R^k)$  satisfying the one-sided boundary condition (31) such that  $\|y^k - y\|_{H^2} + \|R^k - R\|_{L^\infty} + \|\partial_1 R^k - \partial_1 R\|_{L^2} < \delta$ . Set  $n^k := R^k R^\top n$ . Then (31) is satisfied and  $\|\partial_1 n^k - \partial_1 n\|_{L^2} \leq \delta(\|\partial_1 n\|_{L^2} + 1)$ . Since  $\mathcal{E}$  is continuous, (32) follows by choosing  $\delta$  sufficiently small.

Set  $K^k := (R^k)^\top \partial_1 R^k$  and  $U^k = \frac{1}{3}I - (R^k)^\top n^k \otimes (R^k)^\top n^k$ . By Lemma 2.7 and an approximation argument we find  $a^k \in C_c^\infty(\omega)$  and  $\varphi^k \in C_c^\infty(\omega; C^\infty(\bar{S}; \mathbb{R}^3))$  such that

$$\begin{aligned} & \left| \mathcal{E}(y^k, R^k, n^k) - \frac{1}{|S|} \int_{\Omega} Q\left(\bar{x}, \text{sym}(K^k \bar{x} \otimes e_1 + \frac{\bar{r}}{2} \mathbf{1}_{S_0} U^k + (a^k e_1, \bar{\nabla} \varphi^k))\right) dx \right. \\ & \quad \left. - \kappa^2 \int_{\omega} |\partial_1 n^k|^2 dx_1 \right| < \frac{1}{k}. \end{aligned} \quad (33)$$

**Step 2.** (Definition of the recovery sequence).

Let  $y^k, R^k, a^k, \varphi^k$  be as in Step 1, and define for  $h > 0$  the smooth 3d-deformation

$$y_h^k(x) := y^k(x_1) + h R^k(x_1) \bar{x} + h \int_0^{x_1} a^k(s) R^k(s) e_1 ds + h^2 R^k(x_1) \varphi^k(x).$$

A direct calculation yields

$$\begin{aligned} & \frac{R_k^\top \nabla_h y_h^k - I}{h} = K^k \bar{x} \otimes e_1 + (a^k e_1, \bar{\nabla} \varphi^k) + h O_h^k, \\ & \frac{R_k^\top \left( I + \chi_{\Omega_0} (L_h(n^k)^{-\frac{1}{2}} - I) \right) \nabla_h y_h^k - I}{h} = K^k \bar{x} \otimes e_1 + (a^k e_1, \bar{\nabla} \varphi^k) \\ & \quad + \frac{\bar{r}}{2} \chi_{\Omega_0} \left( \frac{1}{3} I - (R^k)^\top n^k \otimes (R^k)^\top n^k + o_h^k, \right. \end{aligned} \quad (34)$$

with remainders  $O_h^k, o_h^k$  satisfying  $\limsup_{h \rightarrow 0} \|O_h^k\|_{L^\infty} < \infty$  and  $\lim_{h \rightarrow 0} \|o_h^k\|_{L^\infty} = 0$ . Hence, by frame-indifference and an expansion at identity we get

$$\begin{aligned} & \lim_{h \rightarrow 0} \left( \frac{1}{h^2 |S|} \int_{\Omega \setminus \Omega_0} W\left(\bar{x}, \nabla_h y_h^k\right) dx + \frac{1}{h^2 |S|} \int_{\Omega_0} W\left(\bar{x}, L_h(n^k)^{-\frac{1}{2}} \nabla_h y_h^k(x)\right) dx \right) \\ & = \lim_{h \rightarrow 0} \left( \frac{1}{h^2 |S|} \int_{\Omega} W\left(\bar{x}, (I + \chi_{\Omega_0} (L_h(n^k)^{-\frac{1}{2}} - I)) \nabla_h y_h^k\right) dx \right) \\ & = \frac{1}{|S|} \int_{\Omega} Q\left(\bar{x}, \text{sym}(K^k \bar{x} \otimes e_1 + \frac{\bar{r}}{2} \mathbf{1}_{S_0} U^k + (a^k e_1, \bar{\nabla} \varphi^k))\right) dx, \end{aligned}$$

and

$$\lim_{h \rightarrow 0} \frac{\kappa^2}{|S_0|} \int_{\Omega_0} |\nabla_h n^k (\nabla_h y_h^k)^{-1}|^2 \det(\nabla_h y_h^k) dx = \kappa^2 \int_{\omega} |\partial_1 n^k|^2 dx_1.$$

Together with (32) and (33) we thus conclude that for any  $\beta \in [0, 1)$ ,

$$\begin{aligned} & \limsup_{k \rightarrow \infty} \limsup_{h \rightarrow 0} \left( \left| \mathcal{E}(y, R, n) - \mathcal{E}_h(y_h^k, n^k) \right| + \|y_h^k - y\|_{L^2} + \|n^k - n\|_{H^1} \right. \\ & \quad \left. + h^{-\beta} \|\nabla_h y_h^k - R\|_{L^\infty} + h^{-\beta} \left\| \frac{(\nabla_h y_h^k)^\top n^k}{|(\nabla_h y_h^k)^\top n^k|} - R^\top n \right\|_{L^\infty} \right) = 0 \end{aligned}$$

We thus obtain the sought for sequence  $(y_h, n_h)$  by extracting a diagonal sequence.  $\square$

#### 4.4 Anchoring – Proof of Proposition 2.3

**Step 1.** (Proof of (a)).

Since  $\mathcal{G}_h$  is non-negative, the conclusion of Theorem 2.1 (a) on compactness remains valid for the modified functional  $\mathcal{E}_h + \mathcal{G}_h$ .

Next we prove the lower-bound: Consider a sequence  $(y_h, n_h) \subset H^1(\Omega; \mathbb{R}^3) \times H^1(\Omega_0; \mathbb{S}^2)$  and  $(y, R, n) \in \mathcal{A}$  such that  $(y_h, \nabla_h y_h, n_h) \rightarrow (y, R, n)$  strongly in  $L^2$ . In view of Theorem 2.1 (b), in order to conclude the claimed lower bound  $\liminf_{h \rightarrow 0} \mathcal{E}_h(y_h, n_h) + \mathcal{G}_h(y_h, n_h; \hat{n}_{bc}) \geq \mathcal{E}(y, R, n) + \mathcal{G}_{\text{weak}}(y, R, n; \hat{n}_{bc})$ , we only need to show that

$$\liminf_{h \rightarrow 0} \mathcal{G}_h(y_h, n_h; \hat{n}_{bc}) \geq \mathcal{G}_{\text{weak}}(y, R, n; \hat{n}_{bc}). \quad (35)$$

W.l.o.g. we may assume that  $\limsup_{h \rightarrow 0} \mathcal{G}_h(y_h, n_h; \hat{n}_{bc}) < \infty$ . Hence,  $f_h := \left| \frac{\nabla_h y_h^\top n_h}{|\nabla_h y_h^\top n_h|} - \hat{n}_{bc} \right|_a \sqrt{\rho}$  defines a bounded sequence in  $L^2$ . Since  $(\nabla_h y_h, n_h) \rightarrow (R, n)$  in  $L^2$  and thus pointwise a.e. (up to extraction of a subsequence), we conclude that  $f_h \rightharpoonup |R^\top n - \hat{n}_{bc}|_a \sqrt{\rho}$  weakly in  $L^2$ . Thus, (35) follows by lower semicontinuity of the convex integral functional  $f \mapsto \int_{\Omega_0} |f|_a^2 \rho dx$  and the definition of  $\mathcal{G}_{\text{weak}}$ .

We finally prove the upper-bound. To that end let  $(y, R, n) \in \mathcal{A}$  and denote by  $(y_h, n_h) \subset H^1(\Omega; \mathbb{R}^3) \times H^1(\Omega_0; \mathbb{S}^2)$  the recovery sequence constructed in Section 4.3 satisfying (30) for some  $\beta \in (0, 1)$ . Moreover, we note that there exists a constant  $C > 0$  (independent of  $h$ ) such that

$$\begin{aligned} & \left| \mathcal{G}_h(y_h, n_h; \hat{n}_{bc}) - \mathcal{G}_{\text{weak}}(y, R, n; \hat{n}_{bc}) \right| \\ &= \left| \int_{\Omega_0} \left( \left| \frac{\nabla_h y_h^\top n_h}{|\nabla_h y_h^\top n_h|} - \hat{n}_{bc} \right|_a^2 - |R^\top n - \hat{n}_{bc}|_a^2 \right) \rho dx \right| \\ &\leq \left( \int_{\Omega_0} \left( \left| \frac{\nabla_h y_h^\top n_h}{|\nabla_h y_h^\top n_h|} - R^\top n \right|_a^2 \right) \rho dx \right)^{\frac{1}{2}} \left( \int_{\Omega_0} \left( \left| \frac{\nabla_h y_h^\top n_h}{|\nabla_h y_h^\top n_h|} + R^\top n - 2\hat{n}_{bc} \right|_a^2 \right) \rho dx \right)^{\frac{1}{2}} \\ &\leq C \left\| \frac{\nabla_h y_h^\top n_h}{|\nabla_h y_h^\top n_h|} - \hat{n}_{bc} \right\|_{L^\infty(\Omega_0)}. \end{aligned} \quad (36)$$

Hence, (30) implies that  $\lim_{h \rightarrow 0} \mathcal{E}_h(y_h, n_h) + \mathcal{G}_h(y_h, n_h; \hat{n}_{bc}) = \mathcal{E}(y, R, n) + \mathcal{G}_{\text{weak}}(y, R, n; \hat{n}_{bc})$  as claimed.

**Step 2.** (Proof of (b)).

Since  $\mathcal{G}_h$  is non-negative, the conclusion of Theorem 2.1 (a) on compactness remains valid for the modified functional  $\mathcal{E}_h + h^{-\beta} \mathcal{G}_h$ .

Next we prove the lower bound. To that end consider a sequence  $(y_h, n_h) \subset H^1(\Omega; \mathbb{R}^3) \times H^1(\Omega_0; \mathbb{S}^2)$  and suppose that  $(y_h, \nabla_h y_h, n_h) \rightarrow (y, R, n)$  strongly in  $L^2$  for some  $(y, R, n) \in \mathcal{A}$ . W.l.o.g. we may assume that  $\limsup_{h \rightarrow 0} \mathcal{E}_h(y_h, n_h) + h^{-\beta} \mathcal{G}_h(y_h, n_h; \hat{n}_{bc}) < \infty$ . Note that this implies that  $\mathcal{G}_h(y_h, n_h; \hat{n}_{bc}) \rightarrow 0$ . Combined with (35) we infer that

$$0 = \mathcal{G}_{\text{weak}}(y, R, n; \hat{n}_{bc}) = \int_{\omega} |R^\top n - \hat{n}_{bc}|_a^2 \bar{\rho} dx_1,$$

and thus  $\mathcal{G}_{\text{strong}}(y, R, n; \hat{n}_{bc}) = 0$ . Hence, Theorem 2.1 (b) yields the claimed lower bound

$$\liminf_{h \rightarrow 0} \mathcal{E}_h(y_h, n_h) + h^{-\beta} \mathcal{G}_h(y_h, n_h; \hat{n}_{bc}) \geq \mathcal{E}(y, R, n) = \mathcal{E}(y, R, n) + \mathcal{G}_{\text{strong}}(y, R, n; \hat{n}_{bc}).$$



We remark that the constructed recovery sequence additionally satisfies the clamped one-sided boundary condition (29).

For the upper bound let  $(y, R, n) \in \mathcal{A}$ . It suffices to construct the recovery sequence in the case  $\mathcal{G}_{\text{strong}}(y, R, n; \hat{n}_{bc}) = 0$ . To that end denote by  $(y_h, n_h) \subset H^1(\Omega; \mathbb{R}^3) \times H^1(\Omega_0; \mathbb{S}^2)$  the recovery sequence of Section 4.3 satisfying (30). Then

$$|h^{-\beta} \mathcal{G}_h(y_h, n_h; \hat{n}_{bc})| = h^{-\beta} |\mathcal{G}_h(y_h, n_h; \hat{n}_{bc}) - \mathcal{G}_{\text{weak}}(y, R, n; \hat{n}_{bc})| \leq Ch^{-\beta} \left\| \frac{\nabla_h y_h^\top n_h}{|\nabla_h y_h^\top n_h|} - \hat{n}_{bc} \right\|_{L^\infty(\Omega_0)},$$

and by (30) we conclude that the right-hand side converges to 0 as  $h \rightarrow 0$ . Hence,

$$\lim_{h \rightarrow 0} (\mathcal{E}_h(y_h, n_h) + h^{-\beta} \mathcal{G}_h(y_h, n_h; \hat{n}_{bc})) = \mathcal{E}(y, R, n) = \mathcal{E}(y, R, n) + \mathcal{G}_{\text{strong}}(y, R, n; \hat{n}_{bc}).$$

We remark that the constructed recovery sequence additionally satisfies the clamped one-sided boundary condition (29).

#### 4.5 Proofs of Lemmas 2.7, 2.9, 2.10, and 2.11

*Proof of Lemma 2.7.* By appealing to  $(\cdot, \cdot)_Q$ -orthogonality and the definition of the orthogonal projections  $P_{\mathbb{H}_{\text{micro}}}, P_{\mathbb{H}_{\text{res}}}, P_{\mathbb{H}_{\text{macro}}}$ , we conclude that

$$\begin{aligned} & \inf_{\chi \in \mathbb{H}_{\text{rel}}} \int_S Q(K\bar{x} \otimes e_1 + \frac{\bar{r}}{2} \mathbf{1}_{S_0} U + \chi) \\ &= \min_{\chi \in \mathbb{H}_{\text{rel}}} \|K\bar{x} \otimes e_1 + P_{\mathbb{H}_{\text{micro}}}(\frac{\bar{r}}{2} \mathbf{1}_{S_0} U) + \chi\|_Q^2 + \|P_{\mathbb{H}_{\text{res}}}(\frac{\bar{r}}{2} \mathbf{1}_{S_0} U)\|_Q^2 \\ &= \|P_{\mathbb{H}_{\text{macro}}}(K\bar{x} \otimes e_1 + \frac{\bar{r}}{2} \mathbf{1}_{S_0} U)\|_Q^2 + \bar{r}^2 E_{\text{res}}(U) \\ &= \|\mathbf{E}(K + \bar{r} K_{\text{pre}}(U))\|_Q^2 + \bar{r}^2 E_{\text{res}}(U) \\ &= \bar{Q}(K + \bar{r} K_{\text{pre}}(U)) + \bar{r}^2 E_{\text{res}}(U). \end{aligned}$$

□

*Proof of Lemma 2.9.* To prove (12), note that by linearity of  $\mathbf{E}$  and the definition of  $\Psi_i$  we have  $\mathbf{E}(K) = \sum_{i=1}^3 k_i \Psi_i$ , and thus

$$\bar{Q}(K) = \left\| \sum_{i=1}^3 k_i \Psi_i \right\|_Q^2 = \sum_{i,j=1}^3 k_i k_j (\Psi_i, \Psi_j)_Q = k \cdot Qk.$$

Next, we prove (13). From the definition of  $Q$  and  $U$  we conclude that

$$(P_{\mathbb{H}_{\text{macro}}}(\mathbf{1}_{S_0} U_j), \Psi_{\hat{i}})_Q = (\mathbf{1}_{S_0} U_j, \Psi_{\hat{i}})_Q = \sum_{i=1}^3 (Q^{-1} U)_{ij} (\Psi_i, \Psi_{\hat{i}})_Q \quad \text{for } \hat{i} = 1, 2, 3.$$

Hence, since  $\{\Psi_1, \Psi_2, \Psi_3\}$  is a basis of  $\mathbb{H}_{\text{macro}}$ , we get

$$P_{\mathbb{H}_{\text{macro}}}(\mathbf{1}_{S_0} U_j) = \sum_{i=1}^3 (Q^{-1} U)_{ij} \Psi_i. \quad (37)$$

In view of the definition of  $K_{\text{pre}}$ , an application of  $\mathbf{E}^{-1}$  to both sides yields

$$K_{\text{pre}}(U_j) = \frac{1}{2} \sum_{i=1}^3 (Q^{-1} U)_{ij} \mathbf{E}^{-1}(\Psi_i).$$

Combined with the definition of  $\Psi_i$ , which yields  $\mathbf{E}^{-1}(\Psi_i) = K_i$ , we conclude  $K_{\text{pre}}(U_j) = \frac{1}{2} \sum_{i=1}^3 (\mathbb{Q}^{-1}\mathbb{U})_{ij} K_i$  and (13) follows by linearity of  $K_{\text{pre}}$ . Finally, we note that in view of orthogonal decomposition  $\mathbb{H} = \mathbb{H}_{\text{res}} \oplus \mathbb{H}_{\text{macro}} \oplus \mathbb{H}_{\text{rel}}$  and (37), we have  $\Phi_j = P_{\mathbb{H}_{\text{res}}}(\mathbf{1}_{S_0} U_j)$ , and thus (14) follows.  $\square$

*Proof of Lemma 2.10.* By the variational characterization of  $P_{\mathbb{H}_{\text{rel}}}$  we have for all  $F \in \mathbb{H}$ ,

$$P_{\mathbb{H}_{\text{rel}}} F = -\chi_F \text{ where } \chi_F \in \mathbb{H}_{\text{rel}} \text{ is characterized by } \|F + \chi_F\|_Q = \inf_{\chi \in \mathbb{H}_{\text{rel}}} \|F + \chi\|_Q.$$

In view of Lemma 2.4 we further conclude that  $\chi_F = (a_F, \bar{\nabla} \varphi_F)$ , where  $(a_F, \varphi_F) \in \mathbb{R} \times H_{\text{av}}^1(S; \mathbb{R}^3)$  is the unique minimizer of the functional (15). Applied with  $F = \mathbf{1}_{S_0} U_j$ , the claimed identity for  $\Phi_j$  follows. The identity for  $\Psi_i$  follows by considering  $F = \text{sym}(K_i \bar{\mathbf{x}} \otimes e_1)$ . Indeed, by definition we have  $\Psi_i = P_{\mathbb{H}_{\text{macro}}}(\text{sym}(K_i \bar{\mathbf{x}} \otimes e_1))$  and since  $\text{sym}(K_i \bar{\mathbf{x}} \otimes e_1) \in \mathbb{H}_{\text{micro}}$ , we conclude (with help of the orthogonal decomposition  $\mathbb{H}_{\text{micro}} = \mathbb{H}_{\text{macro}} \oplus \mathbb{H}_{\text{rel}}$ ) that  $\Psi_j = \text{sym}(K_i \bar{\mathbf{x}} \otimes e_1) - P_{\mathbb{H}_{\text{rel}}}(\text{sym}(K_i \bar{\mathbf{x}} \otimes e_1))$ .  $\square$

*Proof of Lemma 2.11 (a). Step 1.* (Calculation of  $\mathbb{Q}$ ).

We first claim that  $\int_S \bar{\nabla} \varphi_i d\bar{x} = 0$ . To that end consider

$$A := \int_S \bar{\nabla} \varphi_i d\bar{x}, \quad \tilde{\varphi}(\bar{x}) := \varphi_i(\bar{x}) - A\bar{x}.$$

Since  $Q$  is independent of  $\bar{x}$  and  $\int_S K_i \bar{\mathbf{x}} \otimes e_1 d\bar{x} = 0$ , we have

$$\int_S Q(K_i \bar{\mathbf{x}} \otimes e_1 + (a_i e_1, \bar{\nabla} \varphi_i)) d\bar{x} = \int_S Q(K_i \bar{\mathbf{x}} \otimes e_1 + (0, \bar{\nabla} \tilde{\varphi})) d\bar{x} + Q((a_i e_1, A)).$$

By minimality of  $(a_i, \varphi_i)$  we conclude that  $(a_i, A) = 0$  and thus the claim follows.

*Substep 1.1* We prove the formula for  $q_1$  and claim that

$$\Psi_1 = \text{sym} \left( \begin{pmatrix} 0 \\ \frac{x_3}{\sqrt{2}} + \partial_2 \alpha_S \\ -\frac{x_2}{\sqrt{2}} + \partial_3 \alpha_S \end{pmatrix} \otimes e_1 \right).$$

We already now that  $a_1 = 0$  and  $\int_S \bar{\nabla} \varphi_1 d\bar{x} = 0$ . For the argument write  $\varphi_1 = (\alpha, \bar{\varphi})^\top$  and  $\mathcal{K}_1 := \text{sym}(K_i \bar{\mathbf{x}} \otimes e_1)$ . Since  $\text{trace } \mathcal{K}_1 = 0$  a.e. in  $S$ , a direct calculation yields

$$\|\mathcal{K}_1 + \text{sym}(0, \bar{\nabla} \varphi_1)\|_Q^2 = \int_S \frac{\mu}{2} (|\partial_2 \alpha + \frac{x_3}{\sqrt{2}}|^2 + |\partial_2 \alpha - \frac{x_2}{\sqrt{2}}|^2) + \frac{\lambda}{2} (\text{trace } \bar{\nabla} \bar{\varphi})^2 + \mu |\text{sym } \bar{\nabla} \bar{\varphi}|^2 d\bar{x}.$$

Since  $\varphi_1$  is a minimizer, we conclude that  $\bar{\varphi} = 0$  and that  $\alpha$  minimizes (17). Hence,  $\varphi_1 = (\alpha_S, 0, 0)$ . Now, the identities for  $\Psi_1$  and  $q_1$  follow by a direct calculation.

*Substep 1.2* We prove the formulas for  $q_2$  and  $q_3$  and claim that

$$\Psi_2 = \frac{x_2}{\sqrt{2}} \text{diag}(1, -\frac{1}{2} \frac{\lambda}{\lambda + \mu}, -\frac{1}{2} \frac{\lambda}{\lambda + \mu}), \quad \Psi_3 = \frac{x_3}{\sqrt{2}} \text{diag}(1, -\frac{1}{2} \frac{\lambda}{\lambda + \mu}, -\frac{1}{2} \frac{\lambda}{\lambda + \mu}).$$

Indeed, by appealing to the Euler-Lagrange equation one can check that

$$\varphi_2 = -\frac{1}{4\sqrt{2}} \frac{\lambda}{\lambda + \mu} \begin{pmatrix} 0 \\ x_2^2 - x_3^2 \\ 2x_2 x_3 \end{pmatrix} + C_2, \quad \varphi_3 = -\frac{1}{4\sqrt{2}} \frac{\lambda}{\lambda + \mu} \begin{pmatrix} 0 \\ 2x_2 x_3 \\ x_3^2 - x_2^2 \end{pmatrix} + C_3 \quad (38)$$

where  $C_2, C_3 \in \mathbb{R}^3$  are chosen such that  $f_S \varphi_2 = f_S \varphi_3 = 0$ . Now, the identities for  $\Psi_i, q_i$ ,  $i = 2, 3$  follow by direct calculations.

*Substep 1.3* A direct calculation shows that  $\Psi_1, \Psi_2, \Psi_3$  are  $(\cdot, \cdot)_Q$ -orthogonal. Hence,  $\mathbb{Q} = \text{diag}(q_1, q_2, q_3)$  as claimed.

**Step 2.** (Formulas for  $K_{\text{pre}}$ ).

In the isotropic case we have for  $i = 1, 2, 3$  and all  $U \in \mathbb{R}_{\text{dev}}^{3 \times 3}$ ,

$$(\mathbf{1}_{S_0} U, \Psi_i)_Q = \mu \int_S \mathbf{1}_{S_0} U \cdot \Psi_i d\bar{x},$$

since  $\text{trace } U = 0$ . Hence, a direct calculation yields

$$\mathbb{U} = \begin{pmatrix} 0 & \mu \frac{\sqrt{2}}{2} f_S \mathbf{1}_{S_0} (\partial_2 \alpha_S + \frac{x_3}{\sqrt{2}}) d\bar{x} & \mu \frac{\sqrt{2}}{2} f_S \mathbf{1}_{S_0} (\partial_3 \alpha_S - \frac{x_2}{\sqrt{2}}) d\bar{x} & 0 & 0 \\ 0 & 0 & 0 & \frac{\mu(3\lambda+2\mu)}{\lambda+\mu} \frac{1}{2\sqrt{3}} f_S \mathbf{1}_{S_0} x_2 d\bar{x} & 0 \\ 0 & 0 & 0 & \frac{\mu(3\lambda+2\mu)}{\lambda+\mu} \frac{1}{2\sqrt{3}} f_S \mathbf{1}_{S_0} x_3 d\bar{x} & 0 \end{pmatrix},$$

and thus,

$$\mathbb{Q}^{-1} \mathbb{U} = \begin{pmatrix} 0 & \frac{\sqrt{2}}{|S|c_S} \int_{S_0} \partial_2 \alpha_S + \frac{x_3}{\sqrt{2}} d\bar{x} & \frac{\sqrt{2}}{|S|c_S} \int_{S_0} \partial_3 \alpha_S - \frac{x_2}{\sqrt{2}} d\bar{x} & 0 & 0 \\ 0 & 0 & 0 & \frac{2}{\sqrt{3}} \frac{\int_{S_0} x_2 d\bar{x}}{\int_S x_2^2 d\bar{x}} & 0 \\ 0 & 0 & 0 & \frac{2}{\sqrt{3}} \frac{\int_{S_0} x_3 d\bar{x}}{\int_S x_3^2 d\bar{x}} & 0 \end{pmatrix}.$$

□

*Proof of Lemma 2.11 (b).* Since  $S$  is a disc centered at 0, the vector  $(x_3, -x_2)^\top$  is tangential for all  $\bar{x} \in \partial S$  and a short calculation shows that

$$\int_S \left| \begin{pmatrix} \partial_2 \alpha_S \\ \partial_3 \alpha_S \end{pmatrix} + \frac{1}{\sqrt{2}} \begin{pmatrix} x_3 \\ -x_2 \end{pmatrix} \right|^2 d\bar{x} = \int_S |\nabla \alpha_S|^2 + \frac{1}{2} \int_S |(x_3, -x_2)^\top|^2 d\bar{x}.$$

Since  $\alpha_S$  is a minimizer, we conclude  $\alpha_S = 0$ . Now the identities for  $q_1, q_2, q_3$  and  $K_{\text{pre}}$  follow by direct calculations starting from the formulas derived in Lemma (2.11) (a). We note that for  $K_{\text{pre}}$  we also use that  $\int_{S_0} x_2 d\bar{x} = 0$ .

□

## Acknowledgments

The authors acknowledge support by the German Research Foundation (DFG) via the research unit FOR 3013 “Vector- and tensor-valued surface PDEs” (grant no. BA2268/6–1 and NE2138/4–1).

## References

- [AD17a] Virginia Agostiniani and Antonio DeSimone. Dimension reduction via  $\Gamma$ -convergence for soft active materials. *Meccanica*, 52(14):3457–3470, 2017.
- [AD17b] Virginia Agostiniani and Antonio DeSimone. Rigorous derivation of active plate models for thin sheets of nematic elastomers. *Mathematics and Mechanics of Solids*, 2017. doi:10.1177/1081286517699991.

- [ADK17] Virginia Agostiniani, Antonio DeSimone, and Konstantinos Koumatos. Shape programming for narrow ribbons of nematic elastomers. *Journal of Elasticity*, 127(1):1–24, 2017.
- [ALL17] Virginia Agostiniani, Alessandro Lucantonio, and Danka Lučić. Heterogeneous elastic plates with in-plane modulation of the target curvature and applications to thin gel sheets. *arXiv:1706.00629*, 2017.
- [Bar20] Sören Bartels. Finite element simulation of nonlinear bending models for thin elastic rods and plates. In *Handbook of Numerical Analysis*, volume 21, pages 221–273. Elsevier, 2020.
- [BBMN18] Sören Bartels, Andrea Bonito, Anastasia H. Muliana, and Ricardo H. Nochetto. Modeling and simulation of thermally actuated bilayer plates. *J. Comput. Phys.*, 354:512–528, 2018.
- [BBN17] Sören Bartels, Andrea Bonito, and Ricardo H. Nochetto. Bilayer plates: model reduction,  $\Gamma$ -convergent finite element approximation, and discrete gradient flow. *Comm. Pure Appl. Math.*, 70(3):547–589, 2017.
- [BCZ11] Dirk Broer, Gregory P Crawford, and Slobodan Zumer. *Cross-linked liquid crystalline systems: from rigid polymer networks to elastomers*. CRC press, 2011.
- [BGN<sup>+</sup>22] Sören Bartels, Max Griehl, Stefan Neukamm, David Padilla-Garza, and Christian Palus. A nonlinear bending theory for nematic LCE plates. *arXiv preprint arXiv:2203.04010*, 2022.
- [BGNY21] Andrea Bonito, Diane Guignard, Ricardo Nochetto, and Shuo Yang. Numerical analysis of the ldg method for large deformations of prestrained plates. *arXiv preprint arXiv:2106.13877*, 2021.
- [BNS20] Robert Bauer, Stefan Neukamm, and Mathias Schäffner. Derivation of a homogenized bending–torsion theory for rods with micro-heterogeneous prestrain. *Journal of Elasticity*, 141(1):109–145, 2020.
- [BNW20] Juan Pablo Borthagaray, Ricardo H Nochetto, and Shawn W Walker. A structure-preserving FEM for the uniaxially constrained Q-tensor model of nematic liquid crystals. *Numerische Mathematik*, 145(4):837–881, 2020.
- [BP21] Sören Bartels and Christian Palus. Stable gradient flow discretizations for simulating bilayer plate bending with isometry and obstacle constraints. *IMA Journal of Numerical Analysis*, 07 2021.
- [BR20] Sören Bartels and Philipp Reiter. Numerical solution of a bending-torsion model for elastic rods. *Numer. Math.*, 146(4):661–697, 2020.
- [BTW93] P Bladon, EM Terentjev, and M Warner. Transitions and instabilities in liquid crystal elastomers. *Physical Review E*, 47(6):R3838, 1993.
- [BWR<sup>+</sup>08] Miklós Bergou, Max Wardetzky, Stephen Robinson, Basile Audoly, and Eitan Grinspun. Discrete elastic rods. In *ACM SIGGRAPH 2008 papers*, pages 1–12. 2008.
- [CDD02a] Sergio Conti, Antonio DeSimone, and Georg Dolzmann. Semisoft elasticity and director reorientation in stretched sheets of nematic elastomers. *Physical Review E*, 66(6):061710, 2002.

- [CDD02b] Sergio Conti, Antonio DeSimone, and Georg Dolzmann. Soft elastic response of stretched sheets of nematic elastomers: a numerical study. *Journal of the Mechanics and Physics of Solids*, 50(7):1431–1451, 2002.
- [CPB15] Pierluigi Cesana, Paul Plucinsky, and Kaushik Bhattacharya. Effective behavior of nematic elastomer membranes. *Arch. Ration. Mech. Anal.*, 218(2):863–905, 2015.
- [GMAM22] Alain Goriely, Derek E Moulton, and L Angela Mihai. A rod theory for liquid crystalline elastomers. *Journal of Elasticity*, pages 1–24, 2022.
- [KF91] Jürgen Küpfer and Heino Finkelmann. Nematic liquid single crystal elastomers. *Die Makromolekulare Chemie, Rapid Communications*, 12(12):717–726, 1991.
- [KF95] Isabel Kundler and Heino Finkelmann. Strain-induced director reorientation in nematic liquid single crystal elastomers. *Macromolecular rapid communications*, 16(9):679–686, 1995.
- [LTMR92] P Le Tallec, S Mani, and FA Rochinha. Finite element computation of hyperelastic rods in large displacements. *ESAIM: Mathematical Modelling and Numerical Analysis*, 26(5):595–625, 1992.
- [MM03] Maria Giovanna Mora and Stefan Müller. Derivation of the nonlinear bending-torsion theory for inextensible rods by Gamma-convergence. *Calculus of Variations & Partial Differential Equations*, 18(3):287–306, 2003.
- [Neu12] Stefan Neukamm. Rigorous derivation of a homogenized bending-torsion theory for inextensible rods from three-dimensional elasticity. *Archive for Rational Mechanics and Analysis*, 206(2):645–706, 2012.
- [NRV20] Ingo Nitschke, Sebastian Reuther, and Axel Voigt. Liquid crystals on deformable surfaces. *Proceedings of the Royal Society A*, 476(2241):20200313, 2020.
- [NWZ17a] Ricardo H. Nochetto, Shawn W. Walker, and Wujun Zhang. A finite element method for nematic liquid crystals with variable degree of orientation. *SIAM J. Numer. Anal.*, 55(3):1357–1386, 2017.
- [NWZ17b] Ricardo H Nochetto, Shawn W Walker, and Wujun Zhang. A finite element method for nematic liquid crystals with variable degree of orientation. *SIAM Journal on Numerical Analysis*, 55(3):1357–1386, 2017.
- [PKWB18] Paul Plucinsky, Benjamin Kowalski, Timothy White, and Kaushik Bhattacharya. Patterning origami in nematic elastomer sheets. *Bulletin of the American Physical Society*, 2018.
- [PLB18] Paul Plucinsky, Marius Lemm, and Kaushik Bhattacharya. Actuation of thin nematic elastomer sheets with controlled heterogeneity. *Arch. Ration. Mech. Anal.*, 227(1):149–214, 2018.
- [San10] Oliver Sander. Geodesic finite elements for cosserat rods. *International journal for numerical methods in engineering*, 82(13):1645–1670, 2010.
- [SNB16] Oliver Sander, Patrizio Neff, and Mircea Birsan. Numerical treatment of a geometrically nonlinear planar cosserat shell model. *Computational Mechanics*, 57(5):817–841, 2016.

- [vMJZ18] Teunis van Manen, Shahram Janbaz, and Amir A. Zadpoor. Programming the shape-shifting of flat soft matter. *Materials Today*, 21(2):144 – 163, 2018.
- [Wal20] Shawn W Walker. A finite element method for the generalized ericksen model of nematic liquid crystals. *ESAIM: Mathematical Modelling and Numerical Analysis*, 54(4):1181–1220, 2020.
- [WB15] Timothy J White and Dirk J Broer. Programmable and adaptive mechanics with liquid crystal polymer networks and elastomers. *Nature materials*, 14(11):1087, 2015.
- [WBS<sup>+</sup>16] Taylor H Ware, John S Biggins, Andreas F Shick, Mark Warner, and Timothy J White. Localized soft elasticity in liquid crystal elastomers. *Nature communications*, 7(1):1–7, 2016.
- [WT07] Mark Warner and Eugene Michael Terentjev. *Liquid crystal elastomers*, volume 120. Oxford University Press, 2007.